Article

Multiomics dissection of *Brassica napus* L. lateral roots and endophytes interactions under phosphorus starvation

Can Liu[1,2,11], Zhen Bai[1,11], Yu Luo[1,2,11], Yanfeng Zhang[3,11], Yongfeng Wang[4,11], Hexin Liu[1,2,11], Meng Luo[5], Xiaofang Huang[6], Anle Chen[1,2], Lige Ma[1,2], Chen Chen[1], Jinwei Yuan[1], Ying Xu[7], Yantao Zhu[3], Jianxin Mu[3], Ran An[3], Cuiling Yang[4], Hao Chen[4], Jiajie Chen[8], Zaifang Li[8], Xiaodan Li[5], Yachen Dong[5], Jianhua Zhao[5], Xingxing Shen[7,8], Lixi Jiang[7], Xianzhong Feng[8], Peng Yu[6,9]✉, Daojie Wang[4]✉, Xinping Chen[1,2]✉ & Nannan Li[1,2,8,10]✉

Many plants associate with endophytic microbes that improve root phosphorus (P) uptake. Understanding the interactions between roots and endophytes can enable efforts to improve P utilization. Here, we characterize the interactions between lateral roots of endophytes in a core collection of 50 rapeseed (*Brassica napus* L.) genotypes with differing sensitivities to low P conditions. With the correlation analysis result between bacterial abundance and plant physiological indices of rapeseeds, and inoculation experiments on plates and soil, we identify one *Flavobacterium* strain (C2) that significantly alleviates the P deficiency phenotype of rapeseeds. The underlying mechanisms are explored by performing the weighted gene coexpression network analysis (WGCNA), and conducting genome-wide association studies (GWAS) using *Flavobacterium* abundance as a quantitative trait. Under P-limited conditions, C2 regulates fatty acid and lipid metabolic pathways. For example, C2 improves metabolism of linoleic acid, which mediates root suberin biosynthesis, and enhances P uptake efficiency. In addition, C2 suppresses root jasmonic acid biosynthesis, which depends on α-linolenic acid metabolism, improving C2 colonization and activating P uptake. This study demonstrates that adjusting the endophyte composition can modulate P uptake in *B. napus* plants, providing a basis for developing agricultural microbial agents.

Phosphorus (P) is an essential macronutrient for plant growth and development, with important roles in photosynthesis, respiration, reproduction, and other processes[1,2]. Decades of research have shown that P deficiency retards the elongation of primary roots and affects the outgrowth of root hair[3]. Although P is abundant in many soils, the yields of crops planted on 30-40% of arable lands worldwide are negatively affected by an effective soil P deficiency caused by low soluble inorganic phosphate (Pi) contents in the rhizosphere[4–6]. Application of P fertilizer to soils can support plant growth, but this strategy does not necessarily promote P uptake by plants, and can be detrimental to crop yields and the environment[5,7].

The physiological metabolic processes of plants in response to P deficiency depend on the complex regulatory network of P signals. At present, large numbers of transcription factors (TFs), P starvation-

induced genes (PSIs), microRNAs and other functional genes involved in the phospho-signaling regulatory pathway, such as the root cortex cell-located Pi transporter proteins (*PHRs*) of MYB, have been cloned and isolated from *Arabidopsis thaliana*, rice (*Oryza sativa*) and rapeseed (*Brassica napus* L.). The coiled-coil superfamily[8,9], SPX subfamily[10,11], SPX-EXS (PHO subfamily)[12], and the SPX-Major Facilitator Superfamily (SPX-MFS)[13,14] are members of the global transcriptional regulator superfamily (SPX), which greatly promotes researchers' recognition of phosphorus signaling networks.

Rapeseed is a major economic crop with high yields of high-quality oil, accounting for >30% of the world's total plant-based oil production[15,16]. Accordingly, rapeseed quality traits have been a major focus of research. Genome-wide association studies (GWAS) and selective sweeps (such as *Fst*) performed on thousands of different materials (three ecotypes—spring (S), semiwinter (SW) and winter (W)—with different vernalization conditions) collected from all over the world identified many genes related to the regulation of flowering time, abiotic stress response, oil content and quality at the genetic information level[17–19]. The growth of rapeseed plants is sensitive to the availability several crucial chemical elements, such as P deficiency, and the application of P fertilizer can effectively promote plant growth, yield, oleic acid contents and the Pi accumulation in seeds at maturity[20–22]. Overall, rapeseed has become one of the best materials for basic research because of its abundant germplasm resources, wide geographical distribution, and sensitivity to P.

Endophytes may live in plant cells or intercellular spaces and establish a symbiotic relationship with the host plant. Based on their roles in the host plant, endophytes can be divided into mutualistic endophytes (support host growth and development), opportunistic pathogens (causing disease in their plant hosts under certain conditions), and symbiotic endophytes (survival of the endophyte depends on host metabolites without affecting the growth or development of the host)[23,24]. Under natural conditions, symbiotic endophytes can form beneficial symbiotic relationships with many plants and aid in stress responses and growth of the host under nutrient limitation[25,26]. Therefore, research on increasing the rate of nutrient utilization to promote plant growth through the rational deployment of endophytes is important for achieving high yields. For instance, Rho et al. noted that endophyte colonization can effectively enhance the ability of host plants to acclimate to osmotic stress[27]. Plants provide carbon (C) to microorganisms in exchange for nutrients such as nitrogen (N) and P, which can substantially promote the utilization efficiency of soil nutrients by plants[28,29]. For example, arbuscular mycorrhizal fungi (AMF) can enhance plant the growth and development of plants such as potato (*Solanum tuberosum*) and mustard (*Brassica juncea* L.) by improving P uptake to improve abiotic and biotic stress responses and tolerance[30–32]; notably, rapeseed plants do form associations with AMF[33,34]. Research on *Brassica campestris* subsp. *Chinensis* has shown the role of the root-colonizing fungus *Piriformospora indica* in the osmotic stress response and promotion of plant development, particularly in roots, by regulating the balance of phytohormones such as auxin, salicylic acid and jasmonic acid[35–37]. A series of phosphate-solubilizing bacteria in soil, such as *Burkholderia* and *Rhizobia*, have been reported to dissolve Pi by secreting phytic acid or through the action of alkaline phosphatases (*phoA*, *phoD* and *phoX* genes), thus increasing the content of Pi in the soil and improving the uptake of P by plants[38–40]. However, there is a lack of research on endophytic bacteria and whether they can improve the growth of rapeseed plants under P limitation.

To explore the complex interactions between roots and their endophytes in rapeseed plants experiencing P limitation stress, 50 core rapeseed accessions from natural populations, including those of three different ecotypes with relatively distant relatives, were screened in this study. The underground parts of these 50 core rapeseeds, which were planted on soils fertilized (control, CK) or not fertilized (low P, LP)

Table 1 | Comparison of genetic diversity index

Group	N	H_O	H_E	I	PIC (%)	F_{IS}
Spring	15	0.51	0.33	13.23	97.62	−0.35
Semi-winter	8	0.43	0.30	13.23	89.19	−0.24
Winter	27	0.53	0.34	13.24	98.74	−0.40
Mean		0.49	0.33	13.23	95.18	−0.33

N: number of plants; H_O: observed heterozygosity; H_E: expected heterozygosity based on the observed genotype frequencies; I: Shannon-wiener index; PIC: polymorphic information content; F_{IS}: Wright's inbreeding coefficient, significance was determined using the diversity package, after 1000 bootstraps the 95% bias corrected confidence interval was used to determine if the estimated F_{IS} is significantly different from 0.

with phosphatic fertilizer, were collected for transcriptome and amplicon sequencing. Following a correlation analysis between bacterial abundance and plant physiological indices, strain isolation, and functional verification, we identified a *Flavobacterium* strain with the capacity to alleviate P limitation in rapeseed plants. We propose that it is possible to regulate plant growth by changing the composition of symbiotic strains under P limitation conditions to increase the efficiency of P uptake and utilization, thus decreasing the application of P fertilizers and alleviating the pressure of phosphate resources and the ecological environment.

Results

Identification of agronomic trait-related expression modules for low-phosphorus response of 50 core rapeseed cultivars

A total of 272 cultivars with comparatively distant genetic relationships (based on the results of genetic diversity analysis[41]) from a set of 991 accessions collected by Wu[19] were first selected and planted in four plots (50 plants for per cultivar), with two of the plots receiving P fertilizer as control (CK1, CK2), and the other two plots without fertilization treatment for low P conditions (LP1, LP2) (Supplementary Fig. 1). Considering the different vernalization requirements and flowering times of the three ecotypes, the plants samples were selected at the seedling stage (30 days after germination). Finally, 50 core cultivars, comprising 15 S, 8 SW, and 27 W types (Supplementary Fig. 2a), were retained for subsequent sampling by excluding cultivars with inconsistent phenotypes between the two CK plots or the two LP plots. The mean values of observed heterozygosity (H_O), expected heterozygosity (H_E), Shannon–Wiener index (I), polymorphic information content (PIC), and Wright's inbreeding coefficient (F_{IS}) for the three ecotypes were 0.49, 0.33, 13.23, 95.18%, and −0.33, respectively (Table 1), which indicated that these selected rapeseeds had relatively distant genetic relationships. To explore the variation among these 50 cultivars, we performed a principal component analysis (PCA) and phylogenetic and population structure analyses, which revealed that these 50 cultivars cluster into three groups ($K = 3$) that largely correspond to their flowering time habits spring, semiwinter and winter (Supplementary Fig. 2b). Principal component 1 (PC1), explaining 15.1% of the total standing variation, distinguished the spring-type accessions from the semiwinter and winter types, while PC2, explaining 10.8% of the total variation, separated the semiwinter types from the winter types.

Considering the influence of residual phosphorus in the soil on the phosphorus content in roots, the element contents (such as P, copper, iron, potassium, magnesium, manganese, sodium, and zinc) in the aboveground part (shoot) and rhizosphere soil were determined, and shoot (SD) and root (RD) dry weights, the absorption rate of P from soil to shoot (ABS) of these core 50 cultivars were calculated (Supplementary Fig. 3 & Supplementary Data 1). As shown in Fig. 1b, the SD, RD, and P contents in the shoots and the ABS in the LP treatment were significantly lower than those in the CK treatment in S, SW, and W rapeseeds. In addition, *P* was the only element with a
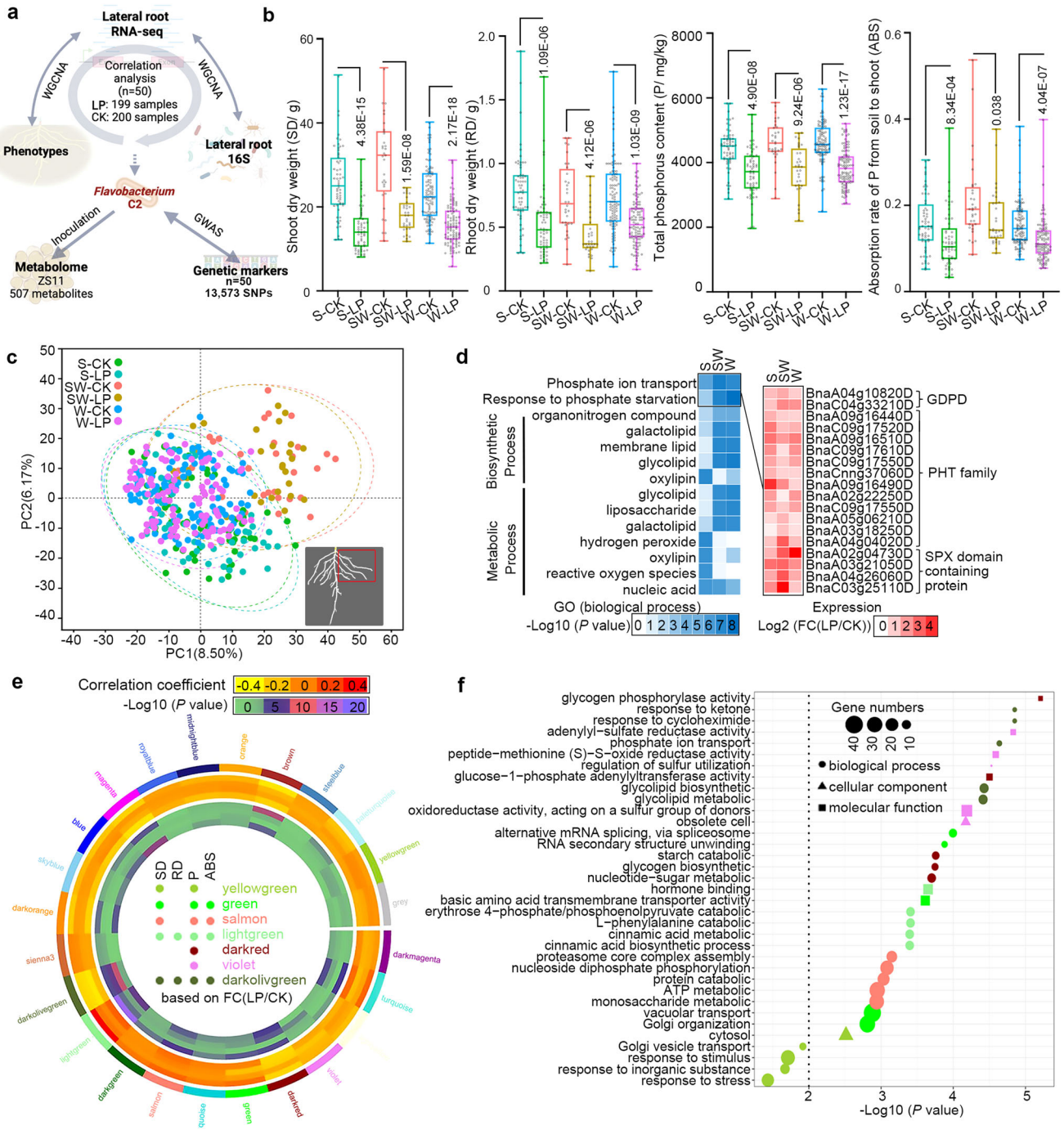
Fig. 1 | Identification of the DEGs associated with phosphorus (P) deficiency.
a Multiple dataset integration analysis of the roots of *Brassica napus* L. This figure was created with https://www.processon.com. **b** Box diagram of shoot dry weight (SD), root dry weight (RD), total phosphorus content (P) and absorption rate of P from soil to shoot (ABS) of three ecotypes under normal and P deficiency conditions. Spring type (S); semiwinter type (SW); winter type (W). Normal control (CK) and P deficiency (LP) groups. A total of 50 cultivars were studied, with 3–4 biological replicates for each cultivar in the CK group (totaling 200 samples) or the LP group (totaling 199 samples). The boxplot displays the median at the center, with the bounds of the box representing the lower quartile (Q1) and upper quartile (Q3). The ends of the whiskers indicate the minimum and maximum values. *P*-values were derived with two-tailed Student's *t*-test. Source data are provided in the Supplementary Data 1. **c** PCA plot of the first two components (PC1 and PC2) of the 399 samples based on the differentially expressed genes (DEGs, log$_2$ (relative expression level) ≥1 and ≤ −1). The red box at the bottom right indicates the

sampled lateral root sampled for RNA-Seq analysis. **d** Gene ontology (GO) term enrichment analysis of the DEGs in three ecotypes associated with P limitation (left), and heatmap representation of the expression of core DEGs related to the P starvation response and P transport (right). In GO enrichment analysis, Fisher's two-tailed test is first conducted, followed by the use of the BH method for multiple testing correction. Source data are provided as a Source Data file. **e** Analysis of module–trait correlations. The involved phenotypes were SD, RD, P and ABS from the outside to the inside. Pearson's correlation coefficient (r) was calculated to evaluate the relationship between the variables, and a two-tailed *t*-test was conducted to obtain the corresponding *P*-value. **f**, GO term enrichment analysis for genes in the violet, dark red, green, salmon, light green, dark olive green, or yellow green modules. Fisher's two-tailed test is first conducted, followed by the use of the BH method for multiple testing correction. The color of the graph corresponds to the color of the module in **e**. Source data are provided as a Source Data file.

significantly different between the LP and CK shoots and rhizosphere soil samples (Supplementary Fig. 3), with a |log$_2$ (LP/CK) | > 0.25 and a *P*-value < 0.05. Subsequently, according to the variation amplitude (sum of log$_2$ (LP/CK)) of these four physicochemical indices of rapeseeds, the sensitivity (emin: R5149, R4247, R4180) or tolerance (with values close to 0 and consistent changes among all four indices: R5124, R4798, R4474) of low P rapeseeds were determined in three ecotypes (Supplementary Fig. 4). To identify the regulatory effects of P limitation on growth and development in the three ecotypes at the transcriptional level, a total of 399 samples (lateral roots from 50 cultivars, 3–4 biological replicates for each plot) were collected for transcriptome deep sequencing (RNA-seq) analysis. The average P contents in the rhizosphere soil of the 50 cultivars growing in the CK or LP plots were 19.46 ppm and 12.52 ppm, respectively (Supplementary Fig. 3). Differentially expressed genes (DEGs) (|log$_2$| (relative expression level) ≥1, padj ≤ 0.05) between these samples were identified according to the RNA-seq data. A PCA of the DEGs indicated some differences in the expression response to P limitation among all three ecotypes (Fig. 1c). A gene ontology (GO) enrichment analysis revealed that the DEGs in the three ecotypes were enriched in biological processes related to phosphate ion transport and response to phosphate starvation (Fig. 1d), such as the glycerophosphodiester phosphodiesterase (GDPD) family, phosphate transporters (PHTs), and other SPX domain-containing proteins. These results provide evidence of the representativeness of rapeseed screening and the effectiveness of the application of P fertilizer in field experiments.

Weighted gene coexpression network analysis (WGCNA) was performed with RNA-seq data and the values for SD, RD, P and ABS to purposefully identify the P stress response-related genes. The dendrogram for the 24 individual modules obtained in this study and genes in the same groups revealed similar trends in expression (Supplementary Fig. 5). The modules were color-coded in relation to the SD, RD, P, and ABS (Fig. 1e). Finally, 7 modules (yellow green, green, salmon, light green, dark red, violet, and dark olive green) were identified (with absolute correlation coefficient values > 0.1 and *P*- value < 0.05), and 5, 2, 7 and 4 of these 7 modules were related to SD, RD, P and ABS, respectively (Fig. 1e & Supplementary Data 2). Agronomic trait-related genes related to the low-phosphorus response were preliminarily identified based on WGCNA. A GO term enrichment analysis of the genes from these 7 module genes indicated that they are significantly enriched in different biological processes, such as response to ketone and cycloheximide, phosphate ion transport, glycolipid biosynthesis and metabolism, and also enriched in molecular functions, such as glycogen phosphorylase and adenylyl sulfate reductase activity (Fig. 1f).

## Microbial co-occurrence and interaction networks in lateral roots

Lateral roots consistent with 399 transcriptomes were collected for microbiome composition analysis via paired-end sequencing of the V3–V4 region of the ribosomal 16S rRNA (16S). A total of 38876 amplicon sequence variants (ASVs) belonging to 545 families and 1,377 genera were identified (Supplementary Data 3). A principal coordinate analysis (PCoA, Supplementary Fig. 6, *P*-value = 0.001), as well as a beta diversity difference analysis (Fig. 2a, *P*-value = 2.561E-40) at the ASV level and analysis of the relative abundances of genera (Fig. 2b) revealed that there were some differences in the responses of all three ecotypes to P limitation. The Wilcoxon rank sum test (corrected for multiple testing with FDR) was performed to evaluate whether there were significant differences in the changes of abundance for the top 17 abundant bacterial genera under LP conditions compared to those detected under CK conditions. The results showed that in the LP environment, the abundances (average in CK or LP) of *Flavobacterium*, *Pseudarthrobacter* and *Stenotrophomonas* decreased, whereas that for *unclassified_f_Comamonadaceae*, *Promicromonospora* and *Pantoea*

increased significantly (Fig. 2c). The ASV abundance of *Flavobacterium* was positively correlated and that of *unclassified_f_Comamonadaceae* and *Promicromonospora* was negatively correlated (|r| > 0.1) with the total P content in the shoots of the rapeseeds (Fig. 2c & Supplementary Fig. 7). Further analysis of these three genera in the three ecotypes revealed that *Flavobacterium* was the only genus that showed the same trends in abundance among the three ecotypes (Supplementary Fig. 8). Considering that the interaction between different microbial strains is a major driving factors of microbial population structure, correlation analysis for these top 17 most abundant bacterial genera was performed to extract their interaction networks in roots, and 46 (4 for *Flavobacterium*) and 48 (6 for *Flavobacterium*) significant correlations (|r| > 0.33, *P*-value < 0.05, drawn by Cytoscape) were detected in the CK and LP samples, respectively (Supplementary Fig. 9, Supplementary Data 4). As one of the hub taxa, *Flavobacterium* was the only member of *Firmicutes* among these 17 genera. The relationships between *Flavobacterium* and other genera in both networks were relatively stable, with positive correlations with *unclassified_f_Oxalobacteraceae* and *Nocardioides*, negative correlations with *Stenotrophomonas* and *Pseudomonas* in both LP and CK conditions, and specific positive correlations with *Massilia* and *unclassified_f_Comamonadaceae* in the LP condition.

To further explore and determine the role of *Flavobacterium* in the P starvation response of its host rapeseeds, correlation analysis revealed 12 gene expression trend modules that were associated with the abundance of *Flavobacterium* |r| > 0.1, *P*-value < 0.05, Supplementary Data 5, with the light green (r = 0.22, *P*-value = 1.39E-05) and dark olive green (r = 0.19, *P*-value = 1.25E-04) modules being consistently associated with both *Flavobacterium* abundance and the four physiological indics (SD, RD, P, ABS; Fig. 2d). Genes in the light green module, such as *4-coumarate--CoA ligase* (*4CL*), *trans-cinnamate 4-monooxygenase* (the cytochrome P450 gene *CYP73A*), *Phenylalanine ammonia-lyase* (*PAL*), *E3 ubiquitin ligase 1* (*SUD1*), *shikimate O-hydroxycinnamoyl transferase* (*HST*) and *Cinnamoyl-CoA reductase 1* (*CCR1*), were enriched in the phenylpropanoid biosynthesis and alpha-linolenic acid metabolism pathways and were significantly downregulated in the three LP samples compared with the CK samples (Supplementary Figs. 10 and 2e). Genes in the dark olive green module were significantly enriched in the glycolysis process, and the expression levels of *Pyruvate kinase* (*PK*), *Phosphofructokinase* (*PFK*), *Glyceraldehyde-3-P dehydrogenase* (*GAPC*), and *Phosphoenolpyruvate carboxylase* (*PPC*) family genes tended to increase in response to low P status (Supplementary Figs. 10 and 2e).
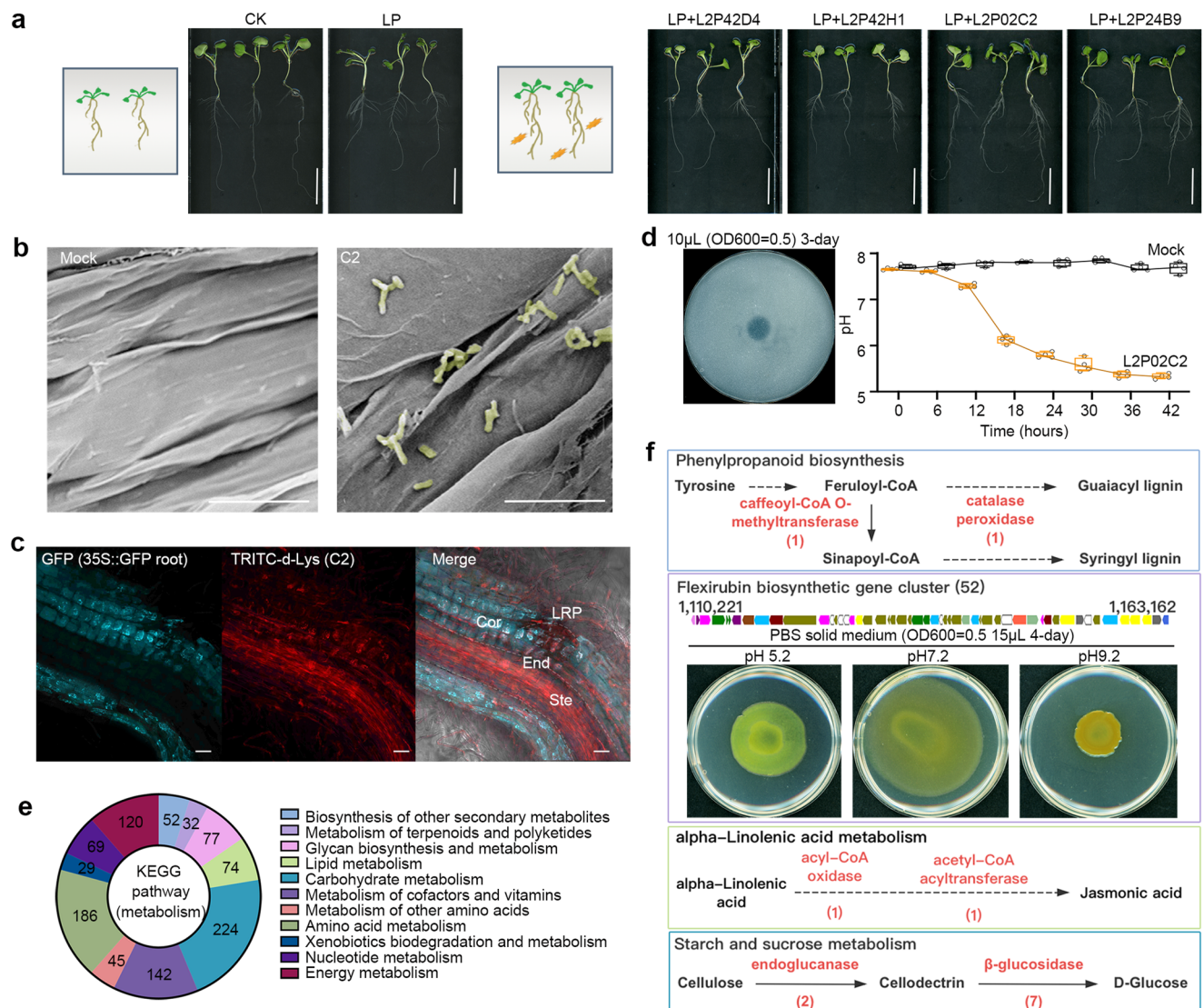
Isolation of core *Flavobacterium* endophytic strains

Four *Flavobacterium* endophytes (L2P42D4, L2P42H1, L2P02C2, and L2P24B9) were purified from the lateral roots of rapeseeds, and identified according to the methods described by Bai et al. (Supplementary Fig. 11)[42]. Plate inoculation assays (using an OD$_{600}$ = 0.5, with an inoculation volume was 1/40 of the medium volume) with these 4 strains showed that 2 or 3 of them can improve the fresh weight of shoots (1.14 – 1.34-fold) or roots (1.06 – 1.45-fold), with only L2P02C2 (C2) could significantly (*P*-value < 0.05) alleviating the retardation of phosphorus starvation on the vegetative growth of Zhongshuang 11 (ZS11) (Fig. 3a and Supplementary Fig. 12); ZS11 is a rapeseed cultivar with a high-quality reference genome that is widely cultivated in China. The lateral roots in the LP (Mock) and LP + C2 (C2) plates shown in Fig. 3a were scanned by scanning electron microscopy (SEM, Fig. 3b), and it was found that C2 cells (diameter, 0.5–1 μm; length, 3–4 μm) can adhere to the surface of the lateral roots. Then, C2 cells labeled with TRITC-d-Lys (Fig. 3c, red) were cocultured with the roots of *35S::GFP* transgenic ZS11 for further colonization verification, and the laser scanning confocal microscopy (LSCM) imaging detected a strong red fluorescent signal in the stele region. Notably, the phosphate solubilizing activity of C2 was identified by halo formation method on
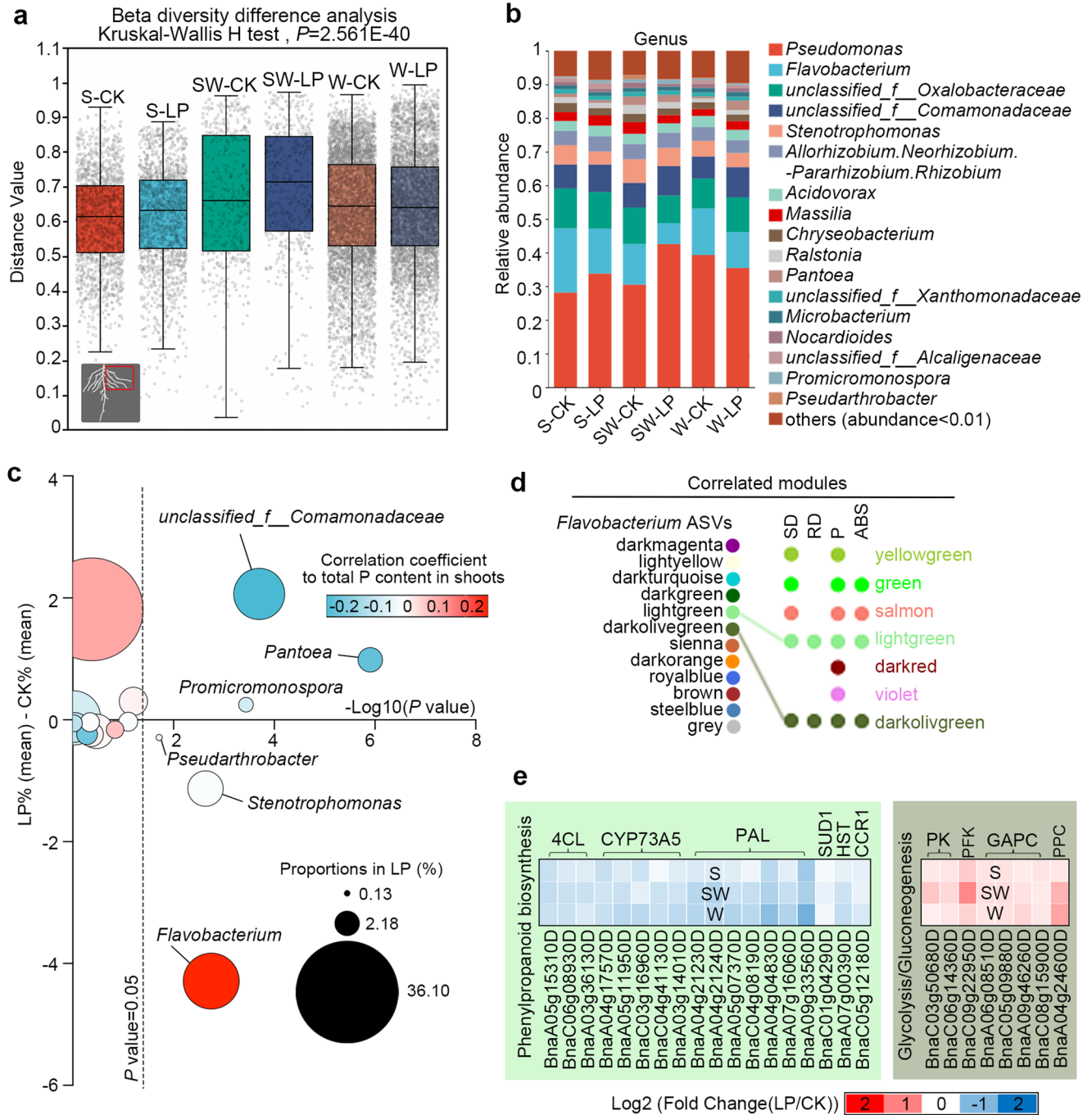
Fig. 2 | Effect of P deficiency on rhizospheric microorganism diversity. a Beta diversity difference analysis results based on the normalized ASV abundance, with the Kruskal–Wallis H test. Normal control (CK) and P deficiency (LP) groups. Spring type (S); semiwinter type (SW); winter type (W). The red box at the bottom left indicates the sampled lateral roots. A total of 50 cultivars were studied, with 3–4 biological replicates for each cultivar in the CK group (totaling 200 samples) or the LP group (totaling 199 samples). Boxplot center: median; box boundaries: lower quartile (Q1) and upper quartile (Q3); minimum: Q1-1.5 × (Q3-Q1); maximum: Q3 + 1.5 × (Q3-Q1). **b** Relative abundance of the 17 most abundant bacterial genera in the CK and LP samples (mean values). The genera with < 1% relative abundance (expressed as the sum of the ASVs across the 399 samples) were classified as "others" (comprising 1360 genera, accounting for 8.2% of all ASVs). Source data are provided as a Source Data file. **c** Correlation analysis of bacterial families as a

function of P content in shoots. The plot shows bacterial families with ≥ 1% relative abundance (17 genera). A two-sided Wilcoxon rank sum test was used for statistical significance and corrected for multiple testing with a FDR, bootstrap = 0.95. The average proportions in LP samples are indicated by circle size. The color of circles denotes the correlation coefficient to the total P content in the shoots. The black dotted line represents the threshold for a *P*-value of 0.05. Source data are provided as a Source Data file. **d** Identification of modules associated with both *Flavobacterium* abundance and four phenotypes (shoot dry weight (SD), lateral root dry weight (RD), phosphorus content (P), and absorption rate (ABS)) based on correlation analysis. **e** Heatmaps representation of gene expression levels for core DEGs associated with phenylpropanoid biosynthesis and glycolysis processes based on the RNA-seq data. Source data are provided as a Source Data file.

Fig. 3 | Isolation of the core *Flavobacterium* associated with the phosphorus starvation response. a Growth status of ZS11 (7 days after germination) on CK, LP, and LP media inoculated with one of four *Flavobacterium* strains. White bars, 3 cm. **b** Scanning electron microscopy images of the lateral root surface of ZS11 grown under mock conditions (left) or inoculated with C2 (right). White bars, 10 µm. The experiment was conducted independently four times, yielding similar results in each case. **c** Colonization patterns of C2 in the roots of ZS11. White bars, 50 µm. Cor, cortex; End, endodermis; Ste, stele; LRP, lateral root primordium. Cyan indicates ZS11 root cells with a GFP signal, and red indicates C2 labeled with TRITC-d-Lys. The experiment was conducted independently three times, yielding similar results in each case. **d** Phosphorus-solubilizing halo on Pikovskaya's solid medium of

Flavobacterium C2 and the pH trend when cultured in Pikovskaya's liquid medium. Four biological replicates were employed. The boxplot displays the median at the center, with the bounds of the box representing the lower quartile (Q1) and upper quartile (Q3). The ends of the whiskers indicate the minimum and maximum values. Source data are provided as a Source Data file. **e** Pie diagram of *Flavobacterium* C2 based on the KEGG annotated gene numbers related to metabolism. Different colors represent different types of metabolites. **f** Schematic diagrams of the key compound biosynthesis clusters or metabolic pathway. The color of each square box corresponds to the KEGG pathway in Fig. 3e. Key enzymes annotated in the C2 genome are shown in red, with the number of enzymes in parentheses. The morphology of the strain on PBS solid media with different pH values are shown.

Pikovskaya's solid medium; moreover, C2 inoculation decreased the pH of the corresponding liquid medium significantly (Fig. 3d). But no potassium solubilization (with no halo on Aleksandrov agar medium) or nitrogen fixation (could not grow on the Azotobacter agar medium) ability was detected.

To investigate the mechanism by which C2 facilitates the vegetative growth of rapeseed plants under low P conditions at the molecular level, a hybrid assembly of Illumina and Nanopore sequencing reads was used to construct a high-quality genome sequence of C2, with a genome size of 4.93 Mb and a CDS number of 4363 (Supplementary Fig. 13), including 1050 genes involved in various metabolic reactions (Fig. 3e). Kyoto encyclopedia of genes and genomes (KEGG) annotation information about the metabolites indicated that C2 may

play a role in the biosynthesis of phenylpropanoids (with one gene encoding caffeoyl-CoA O-methyltransferase and on encoding catalase peroxidase), flexirubin-type phytochromes (forming a cluster with 52 genes) and the metabolism of alpha-linolenic acid (one caffeoyl-CoA O-methyltransferase, and one catalase peroxidase), starch and sucrose (two genes encoding endoglucanases and seven genes encoding beta-glucosidases) (Fig. 3f and Supplementary Data 6). The strain was light yellow when growing on acidic medium (pH 5.2) and orange on alkaline medium (pH 9.2), which was consistent with the presence of the flexirubin biosynthesis-related gene cluster in the C2 genome (Fig. 3f). C2 belongs to *Flavobacterium* genus, and a phylogenetic tree with related bacteria showed that C2 is close to *Flavobacterium sharifuzzamanii* strain A7.6 T (*Flavobacterium* _sp003254585|

GCF_003254585.1; Supplementary Fig. 14), with an 88.99% average nucleotide identity (ANI) value, indicating that C2 and A7.6 T belong to different species. Based on the 16S data, a total of 1,586 *Flavobacterium* ASVs (sum of all reads: 967,301) were identified (Supplementary Data 7), of which 166 ASVs had an average read > 1 among the 399 16S samples. ASV195, which had the highest relative abundance (18.26%), showed 96.486% identity with the 16S rRNA sequence of C2 (*e*-value = 8.24E − 176). ASV5102 shared 100% identity with the 16S rRNA sequence of C2, but with low abundance (0.32%) and prevalence (6.677%). In addition, 48 of the 166 ASVs were highly consistent with the 16S rRNA sequence of C2 (Supplementary Data 8, *e*-value = 0, identity > 97.297%), with an abundance accounting for 19.71% of the total (sum reads: 190,643) and high prevalence (99.499%). The abundance of these 48 ASVs in LP sample was 13.3% lower than that of CK sample (*P*-value = 0.0222), which was consistent with the decreasing trend of *Flavobacterium* abundance shown in Fig. 2c. These results therefore indicate that although C2 isolated in this study is not the dominant endophytic *Flavobacterium* in terms of abundance in rapeseed lateral roots, strains with similar functionalities as C2 are important components of the endophytic *Flavobacterium* population in rapeseed roots.

Functional characterization of *Flavobacterium* C2

To investigate how C2 is involved in the effects of phosphate starvation on rapeseed growth and development, ZS11 and 6 representative rapeseed cultivars (Supplementary Fig. 4, highlighted with red text) were subjected to soil culture experiments (Fig. 4a). When grown under LP conditions, the fresh weights of the shoots and roots of these 7 cultivars decreased to different extents compared to those measured under CK conditions; the relative change seen for the low-P-sensitive cultivars (R5149, R4247, and R4180) was relatively greater than that for the more tolerant cultivars, consistent with the data shown in Supplementary Fig. 4. Notably, the fresh weights of their shoots and roots increased in response to C2 inoculation, especially in R5149 (Fig. 4b). Furthermore, CK and LP (with 625 µM or 12.5 µM KH$_2$PO$_4$ added to the 1/2 MS base salts (-P, without vitamins)) plate experiments were performed with ZS11 and R5149, and C2 inoculation (OD$_{600}$ = 0.5, the inoculation volume was 1/40 of the medium volume) resulted in better growth of both (Fig. 4c). These results indicate that C2 colonization of the root system of rapeseed seedings can significantly improve their growth under P-limited conditions, especially in low-P-sensitive cultivars. Then, ZS11, which has a high-quality reference genome and already produced desirable results in the inoculation experiments, was selected for additional determination of its substance content. The lateral roots of the corresponding material shown in Fig. 4b (ZS11, LP and CK; inoculated with the C2 strain or not, three biological replicates) were used for the determination of the quasi-targeted metabolome. A PCA of these four groups of samples using their differentially abundant metabolites (variable importance in the projection, VIP > 1.0, FC > 1.2 or FC < 0.833, *P*-value < 0.05) revealed that inoculation with C2 significantly changed the metabolite composition of seedings in response to low P stress (Fig. 4d). KEGG pathway enrichment analysis indicated that C2 inoculation of seedlings grown under LP conditions decreases the abundance of metabolites involved in glycolysis, fructose and mannose metabolism, starch and sucrose metabolism, and ubiquinone biosynthesis but led to a rise in the levels of phenylalanine, biotin, glycerolipids, linoleic acid, and alpha-linolenic acid and the biosynthesis of phenylpropanoids and terpenoid backbones, among other compounds (Fig. 4d, Supplementary Data 9 & 10). More sucrose was specifically accumulated in the roots after the treatment with C2 under LP conditions, and then the intermediate metabolites were transferred to oxaloacetate and entered the tricarboxylic acid (TCA) cycle or the glyoxylate and dicarboxylate metabolism pathway (Fig. 4e). Staining with Lugol's solution confirmed the greater starch accumulation in the ZS11 lateral root tips of

the LP samples than in those of the CK and LP + C2 samples (Fig. 4f). These results are consistent with the functions of the genes in the two core modules (light green and dark olive green) shown in Fig. 2d resulting from the WGCNA. Finally, RT–qPCR was used to verify the expression levels of five key genes. The expression of GDP-D-mannose 4,6-dehydratase 1 (*GMD1*, *BnaA07g15220D*), a gene in the light green module, was repressed, whereas the expression of four genes in the dark olive green module, namely, two *GAPC* genes (*BnaC05g09880D/BnaA09g46260D*), one *PK* gene (*BnaC06g14360D*) and one *PPC2* gene (*BnaA04g24600D*), were upregulated under P limitation and aseptic conditions (Fig. 4e). C2 inoculation led to greater amplitude in the expression changes seen for these five genes under LP conditions. Taken together, these results indicate that C2 inoculation can mitigate the starch accumulation caused by growth under LP conditions in rapeseed roots, ensuring that a sufficient amount of substrate enters the TCA cycle through the glycolysis pathway.

Identification and validation of core genes associated with lipid metabolism-mediated suberin and jasmonic acid biosynthesis

Genome-wide association studies (GWAS) were performed on the variation in the abundance of the ASV (in the lateral roots of 50 core cultivars, with 13,573 SNPs) of *Flavobacterium* in the LP treatment relative to that in the CK treatment (with the value of log$_2$ (fold-change [average LP1, LP2/average CK1, CK2])) (Fig. 5a and Supplementary Fig. 15). A total of 221 genes were identified with the online page server BnaGWAS (Supplementary Data 11). Two genes in the light green module overlapped with the 221 GWAS-associated genes, including one *CCR1* gene (*BnaC05g12180D*, involved in lignin biosynthesis). Furthermore, other genes whose homologs in *Arabidopsis* play roles in lignin and suberin biosynthesis and the jasmonic acid (JA) signaling pathway[43–46] were also present in the region with significant association signals. These genes included one ATP-binding cassette (ABC) transporter G family member (*ABCG2*, *BnaA04g21360D*, encoding a suberin monomer transporter), one cytochrome P450 gene (*CYP86B1*, *BnaA09g01800D*, mediating fatty acid hydroxylation and oxidation from ω-hydroxy fatty acids to α, ω- dicarboxylic acids), one 3-ketoacyl-CoA synthase gene (*KCS20*, *BnaC07g17300D*, controlling the elongation of long-chain fatty acid precursors), and one jasmonate ZIM domain-containing gene (*JAZ13*, *BnaCnng69490D*, encoding a repressor of JA signaling), (Fig. 5a). Notably, C2 inoculation specifically affected phenylpropanoid biosynthesis and linoleic acid and alpha-linolenic acid metabolism in the lateral roots of ZS11 seedings grown under LP conditions compared to that under the CK conditions (Fig. 4d). These substances are involved in alpha-linolenic acid metabolism-mediated root JA, suberin and lignin biosynthesis.

To validate the above changes in expression obtained by RNA-seq, we chose nine genes related to these biosynthesis pathways and affected by LP treatment and C2 inoculation from the light green module of WGCNA (Fig. 2e & Supplementary Fig. 10) or annotated by GWAS (Fig. 5a) to check their expression patterns by RT–qPCR. These nine genes included seven genes from the suberin and lignin biosynthetic pathways (two *PAL2* genes and one gene each of *CYP73A5*, *4CL1*, *CCR1*, *KCS20*, *CYP86B1*), the suberin monomer transporter gene *ABCG2* and the JA signaling repressor gene *JAZ13* (Fig. 5b; green and purple points). In addition, the contents of key chemicals in the relevant pathways were determined via metabolic analysis, including alpha-linolenic acid, linoleic acid, JA, four common intermediates of the lignin or suberin biosynthesis pathway (L-phenylalanine, coumaric acid, caffeic acid, and ferulic acid) and three lignin substrates (sinapyl alcohol, coniferyl alcohol, and p-coumaryl alcohol). The expression levels of all 9 genes decreased in response to LP, as did the accumulation of JA and the decreases in caffeic acid, sinapyl alcohol, and p-coumaryl alcohol (Fig. 5b, |FC| > 0.5). C2 inoculation increased the expression levels of genes form the suberin and lignin biosynthetic pathways and of *ABCG2* in the LP conditions. Moreover, the contents of
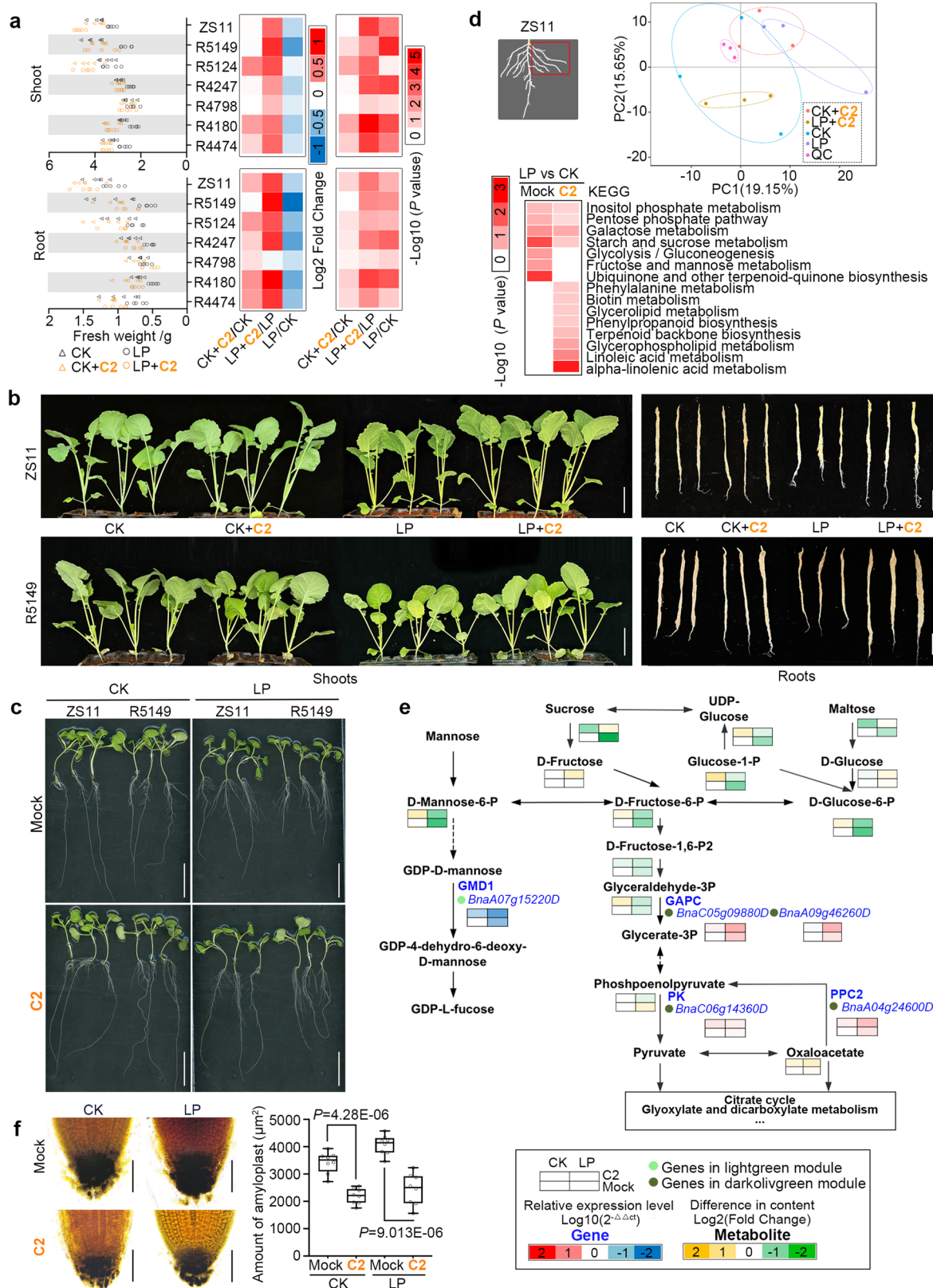
L-phenylalanine, coumaric acid, ferulic acid, alpha-linolenic acid, linoleic acid and JA decreased after C2 inoculation, whereas the contents of coniferyl alcohol and p-coumaryl alcohol increased under the same conditions (Fig. 5b). These results suggest that under LP conditions, more JA accumulates derived from alpha-linolenic acid metabolism, whereas the biosynthesis of suberin in rapeseed roots

decreases due to metabolic flux rearrangement. However, inoculation with C2 resulted in the resumption of suberin biosynthesis and transport, and the mitigation of JA biosynthesis induced under LP conditions.

Suberin deposition along the endodermis of the primary root follows a typical pattern with three zones from the root tip to the

Fig. 4 | Functional identification of *Flavobacterium* C2. a Statistical results of the fresh weight of shoots or roots of ZS11 and the other 6 core rapeseeds planted in soils inoculated with or without C2. CK, 625 µM P; LP, 12.5 µM P. *P*-values were derived with two-tailed Student's *t*-test. Five seedlings per genotype and conditions were used. Source data are provided as a Source Data file. **b** Growth status of 21 day-old ZS11 and R5149 plants planted in soil inoculated with or without C2. White bars, 5 cm. The leaves are shown on the left, and the corresponding root systems are shown on the right. **c** Growth status of R5149 and ZS11 (7 days after germination) on sterile 1/2 MS medium inoculated (C2) or not (Mock) with C2. White bars, 3 cm (**d**) PCA plot of the root samples in Fig. 4b based on the differentially abundant metabolites (variable importance in the projection (VIP) > 1.0, FC > 1.2 or FC < 0.833, *P*-value < 0.05). KEGG enrichment analysis of the differentially abundant metabolites. Fisher's two-tailed test is first conducted, followed by the use of the BH method for multiple testing correction. The red box at the bottom right indicates

the sampled lateral root. Source data are provided as a Source Data file. **e** Expression verification of core genes (based on the RT–qPCR results, the expression levels were normalized to that of *ACT7*) and the changes in the contents of key metabolites (based on the metabolome data) in the soil culture materials in the glycolytic pathway. Key genes are shown in blue. The black letters indicate key metabolites. All data were compared against the samples marked with red dots in the diagram. Three biological replicates were used in these experiments, with 5 plants per biological replicate. Source data are provided as a Source Data file. **f** Amyloplast staining with Lugol's solution and number of amyloplasts in ZS11 lateral root tips. Black bars, 50 µm. Eight biological replicates were employed. The boxplot displays the median at the center, with the bounds of the box representing the lower quartile (Q1) and upper quartile (Q3). The ends of the whiskers indicate the minimum and maximum values. *P*-values were derived with two-tailed Student's *t*-test. Source data are provided as a Source Data file.

shoot: the non-suberized, patchy suberized and fully suberized zones in *Arabidopsis*[47]. The primary roots of ZS11 seedings in Fig. 4b were stained with Fluorol Yellow 088 and there was no significant change in the proportion of the suberized zone, but there was a significant difference in the fluorescence intensity at 1.5 cm from the root tip (Supplementary Fig. 16). Indeed, compared to that in the CK treatment, the accumulation of suberin in the LP treatment decreased, while C2 inoculation significantly restored the suberin content in the LP treatment (Supplementary Fig. 16). Furthermore, lignification (as estimated by basic fuchsin staining) increased in LP treatment and then decreased with C2 inoculation (Supplementary Fig. 16). Fluorol Yellow 088 staining of the third lateral roots of ZS11 also revealed that the proportions of the non-suberized and patchy suberized zones significantly increases in the LP samples, whereas C2 inoculation increased the proportions of these zones (Fig. 5c). Linolenic acid also plays an important role in JA biosynthesis. Quasi-targeted metabolomics analysis showed that JA content significantly increases under P limitation conditions and that C2 inoculation decreases the JA biosynthesis rate in rapeseed roots (Fig. 5b). The JA content of the lateral root samples in Fig. 4b was further quantified by LC–MS/MS analysis (Fig. 5d), and the change trend was consistent with that shown in Fig. 5b.

Interestingly, two key rate-limiting enzymes in JA biosynthesis pathways: acetyl-CoA oxidase (ACX, gene2745) and acetyl-CoA acyltransferase (ACAA, gene4100) were annotated in the C2 genome. Two homologous genes with the highest relative expression abundance in the rapeseed genome were selected for an RT–qPCR analysis (Fig. 5b; blue points). C2 inoculation significantly decreased the expression levels of *ACX2s* (*BnaA09g07080D*, *BnaC09g06780D*) and *ACAA2s* (*BnaC04g11470D*, *BnaA03g15290D*) in seedlings experiencing P limitation. Then, Col-0 and the double mutant *acx2-1/3-6*[48] were planted on plates containing 250 µM P (CK), 10 µM P (LP Mock), or 10 µM P with C2 inoculation (LP + C2), or 10 µM P with C2 inoculation and 5 µM MeJA treatment (LP + C2+MeJA). As shown in Supplementary Fig. 17, the root length of *acx2-1/3-6* seedings in the CK condition was similar to that of Col-0 but shorter than that in the LP condition. C2 inoculation on the LP plate effectively increased root development, but additional application of MeJA significantly inhibited root development in both Col-0 and *acx2-1/3-6* seedings. Overall, the application of C2 regulates the suberin distribution in the roots and inhibits the biosynthesis of JA under P limited conditions, which may improve the efficiency of P uptake and vegetative growth of rapeseed roots.

Discussion
Selection of representative rapeseed cultivars and effectiveness of low-Pi treatment
In this study, 272 cultivars with relatively distant relatives were initially selected from 991 accessions collected by Wu[19] based on the results of genetic diversity analysis. Then, 50 cultivars with significant differences in P content (aboveground) and dry weight (aboveground and

underground) between CK and LP were selected as the key objects of this study. PCA or beta diversity difference analysis of the three ecotypes based on RNA-seq or 16S data revealed significantly different expression profiles and endophytic components in lateral roots between CK and LP conditions (Figs. 1c & 2a). The GO classifications in Fig. 1d were also enriched in phosphate ion transport and in response to phosphate starvation. All these results are evidence of the representative nature of the rapeseed cultivars chosen for this study and of the effectiveness of the application of P fertilizer in field experiments.

Phosphate-solubilizing bacterium C2
The known mechanisms of phosphate solubilizing bacteria (PSB) mainly include organic acid acidolysis and enzymatic hydrolysis[49]. The organic acids produced by PSB include gluconic acid, oxalic acid, malic acid, and citric acid[50]. Moreover, rhizosphere acidification may increase the bioavailability of slightly dissolved mineral P (such as calcium phosphate) to plants[51]. The C2 genome encodes one citrate synthase gene (gene0379) and one aconitate hydratase gene (gene1974) for citric or isocitric acid synthesis, one malate dehydrogenase gene (gene2207) for malic acid biosynthesis, and one aldehyde dehydrogenase gene (gene3047) for acetic acid biosynthesis. A metabolite analysis indicated that the contents for some organic acids did not vary significantly in the lateral roots of rapeseed seedlings, regardless of their inoculation with C2 (Supplementary Fig. 18). However, C2 did decrease the pH in insoluble phosphorus media during reproduction (Fig. 3d). This may be related to organic acids being secreted into the soil and excess organic acids in plants being used as substrates for other reactions. Overall, the ability of C2 to dissolve P is due to its ability to produce acid, which is similar to that of *Flavobacterium sharifuzzamanii* strain A7.6 T[52]. Partial PSBs not only provide available P to plants but also secrete auxins and other plant growth regulators to promote plant growth. Three aldehyde dehydrogenase genes (*ALDH*, gene1196/3391/4067) for IAA biosynthesis were annotated in the C2 genome. Metabolomic data revealed that the IAA content decreased (0.76-fold) under LP stress without C2 inoculation but increased (1.58-fold) with C2 inoculation. In addition, C2 formed a pink color when added to the Salkowski colorimetric solution (Supplementary Fig. 19), and the yield of IAA in the fermentation broth was 1.40 ± 0.20 mg/L after culture at 28 °C for 7 days. These results demonstrate the ability of C2 to produce IAA. In summary, C2 can produce organic acids and IAA, two beneficial substances that promote vegetative growth in its host.

Flavobacterium C2 participates in the regulation of carbohydrate biosynthesis and metabolism
P plays an important role in carbohydrate metabolism and is directly involved in starch and sucrose metabolism, glycolysis and other metabolic pathways[53]. Therefore, changes in carbohydrate metabolism are a universal response under low P conditions, with most plants showing a general increase in starch and a decrease in sucrose
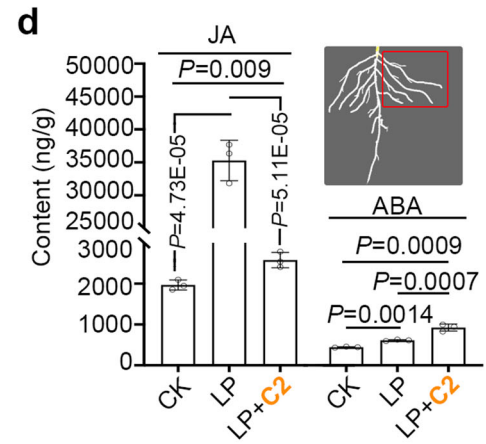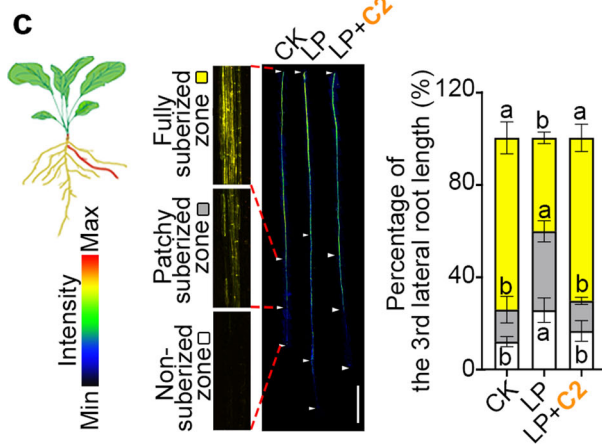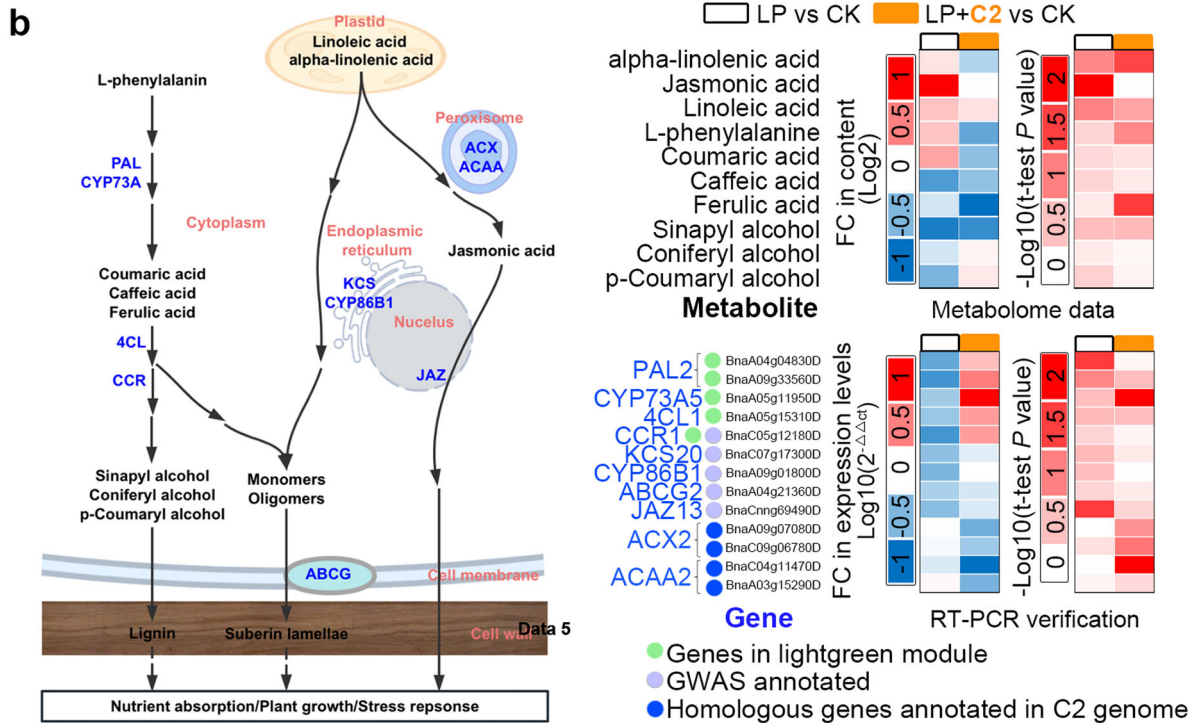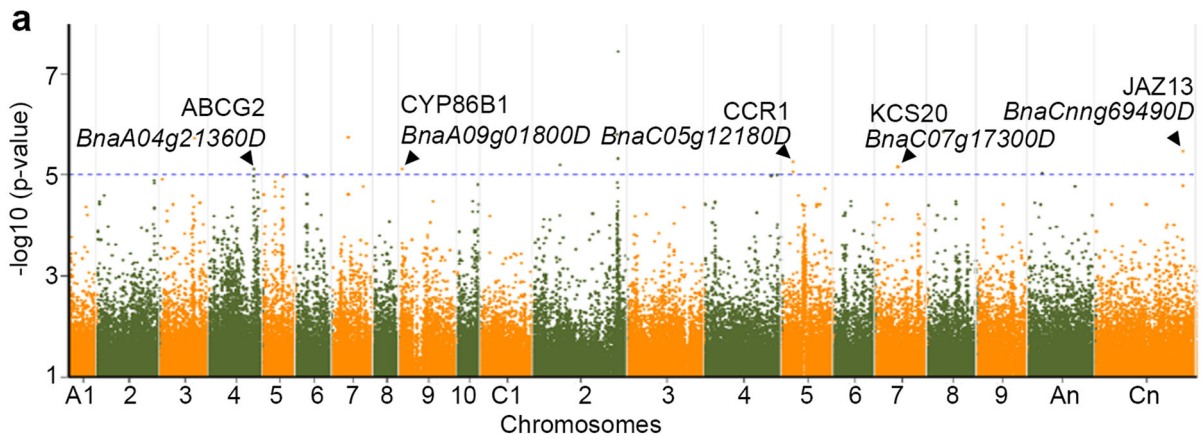
contents[6,54]. Li et al. used transcriptome and physiological studies to confirm the involvement of plant hormones and sugars in the P starvation response of rapeseed[55]. Genes encoding proteins such as sucrose-phosphate synthase-like protein and 6-phosphogluconate dehydrogenase were differentially expressed between the LP-tolerant rapeseed line 102 and the LP-sensitive rapeseed line 105

during growth under LP conditions[56]. The induction of *BnPht1;4* expression, a crucial phosphate transporter gene, by P limitation conditions depends on the presence of sugar[57]. In this study, both the gene functions in the light green and dark olive green modules and metabolome data indicated that C2 inoculation influenced carbohydrate biosynthesis and metabolism in the lateral roots of rapeseed

Fig. 5 | Effect of *Flavobacterium* C2 on fatty acid metabolism in rapeseed. a Manhattan plot of the association signal for ASV abundance variation of *Flavobacterium* in LP relative to CK, based on genome-wide SNPs. The horizontal dashed lines indicates the genome-wide significance thresholds ($-\log10$ (P-value) = 5). P-values for SNPs were calculated using the EMMAX model based on the chi-squared distribution, followed by the application of the Benjamini-Hochberg method to correct for multiple testing. **b** Heatmap representation of the changes in key metabolite contents (based on the metabolome data) and core gene expression levels (based on RT–qPCR, normalized to *ACT7*) in the soil culture materials related to α-linolenic acid metabolism-mediated root jasmonic acid synthesis. Key genes are shown in blue; key metabolites are shown in black; cell structures are shown in red. FC, fold change. P-values were derived from two-tailed Student's *t*-test. Three

biological replicates were used in these experiments, with 5 plants per biological replicate. Source data are provided as a Source Data file. This figure was created with https://www.processon.com. **c** The different depositions of suberized zones in the third lateral root of ZS11 in Fig. 3b. White bars=1 cm. The values represent the means ± SDs. Different letters represent significant differences among groups (one-way ANOVA, followed by Duncan's test, P-value < 0.05). Five plants were used in the experiment. The white arrows mark the beginning and end of each root zone. Source data are provided as a Source Data file. **d** JA and ABA contents. P-values were derived from a two-tailed Student's *t*-test. Three biological replicates were used in these experiments, with 5 plants per biological replicate. The values represent the means ± SDs. The red box at the bottom right indicates the sampled lateral root. Source data are provided as a Source Data file.

seedings. As shown in Fig. 4e, the levels of sucrose, maltose, D-mannose-6-P, D-glucose-6-P, and D-fructose-6-P decreased, whereas the levels of GDP-L-fucose and phosphoenolpyruvate significantly rose under LP conditions in the absence of C2. However, C2 inoculation significantly increased the contents of sucrose and maltose in rapeseed lateral roots under LP conditions. As the main source of energy in plants, glucose is used in large quantities in response to stressful environments[58], and double sugar molecules (i.e., disaccharides, such as sucrose and maltose) are preferentially hydrolyzed to guarantee a steady supply of glucose and provide energy[59]. The C2 genome contains two endoglucanase genes (gene0759, gene4324) and seven beta-glucosidase genes (gene0760, gene1555, gene2620, gene2748, gene 3461, gene 3563, gene 4339)[60,61]. Presumably, the nine enzymes encoded by these key genes enable C2 to colonize roots, degrade cellulose, and provide the host with a certain amount of glucose, which subsequently diminishes the host consumption of its own disaccharides, resulting in a relative increase in sucrose, maltose, fructose contents under LP conditions. Eventually, relatively sufficient amounts of the substrates likely enter the TCA cycle via the glycolysis pathway to produce more energy, or more oxaloacetate, an important precursor, which will enter the glyoxylate and dicarboxylate metabolism pathways to produce organic acids[62]. The upregulated expression levels of the genes encoding the rate-limiting enzymes GAPC, PK and PPC2 after C2 inoculation are also consistent with this hypothesis. Thus, in general, C2 inoculation can effectively alleviate the constraints imposed by LP stress on host vegetative growth by replenishing carbon sources to the host.

Flavobacterium C2 affects the biosynthesis of suberin and jasmonic acid in rapeseed

Limited availability of nutrients can activate multiple responses, such as altering the development of Casparian bands (CBs) and suberin lamellae (SLs), which are composed mainly of suberin and lignin and are crucial for selective nutrient uptake[63–66]. However, it is important to note that the deposition of suberin and lignin in roots responds differently to the type of nutritional limitation or plant hormone levels[64]. For example, a decrease in suberin in the root endodermis of barley (*Hordeum vulgare*) plants can limit nutrient loss and favor the inward radial transport of calcium and sodium[67]. The lignification of CB was enhanced in barley roots experiencing LP conditions[68]. Schneider et al. reported that root cortical senescence (RCS) decreased phosphate transport in nodal roots but coincided with increased suberin in the endodermis of barley[69]. The expression of members of the cytochrome P450 and omega-hydroxypalmitate O-feruloyl transferase gene families, which are involved in the biosynthesis of suberin, were highly upregulated in the LP-tolerant *indica* rice cultivar Chakhao Poreiton[70]. As shown in Figs. 5c and S16, less suberin was deposited in both the primary and lateral root endodermis when ZS11 was grown on LP soil, whereas more suberin deposition was detected after C2 inoculation; the lignin content showed an opposite trend to that of suberin. Moreover, the staining patterns for suberin and lignin are consistent with the expression or contents of the key genes and intermediate

metabolites shown in Fig. 5b. Given that *ABCG2* (a suberin monomer transporter gene) was previously reported to be correlated with the P content in rapeseeds[71], the P content was determined with the ZS11 materials shown in Fig. 4b. It was found that C2 inoculation significantly increased the P content in the aboveground part of ZS11 under LP conditions (Supplementary Fig. 20). These results suggest that suberin-mediated cell wall modification appears to be important for improving LP stress tolerance in rapeseed, and that C2 colonization can promote the utilization of P by the root of rapeseed seedlings via suberin biosynthesis and resumption of P transport.

Linolenic acid also plays a role in JA biosynthesis, and the JA content has been reported to increase in response to LP stress by the upregulating the expression of genes encoding allene oxide cyclase (AOC), allene oxide synthase (AOS), and other gene products in *Arabidopsis*[6,72]. As shown in Fig. 5b and d, the JA content was significantly increased under LP conditions but decreased upon C2 inoculation in the roots of rapeseed seedings. Moreover, C2 inoculation did not increase the P content of the roots (Supplementary Fig. 21). This finding suggests that the change in P content in the roots is not the most important factor in the decreased JA content after inoculation with the phosphate-soluble bacterium C2. These results may be related to the presence of one *ACAA* gene and one *ACX* gene in the C2 genome, encoding two of the key rate-limiting enzymes in the JA biosynthesis pathway. The sequence of *ACAA* in the C2 genome is highly similar to that of *KAT2* in *Arabidopsis*, which plays a role in peroxisomal β-oxidation, such as that of fatty acids and the jasmonate precursor oxophytodienoic acid[73], and contributes to wounding-induced JA production[74]. The C18:3n3 (linolenic acid) content in the *kat2-5* mutant was reported to be lower than that in the wild-type Col-0[73], which was consistent with the decreased expression levels of *ACAA2* family members in rapeseeds and the decreased linoleic acid content in LP + C2 samples compared with LP samples (Fig. 5b). The sequence of *ACX* in the C2 genome is highly similar to that of *ACX2* and *ACX3* in *Arabidopsis*, which are involved in JA production in pathogen-infected plants[75–77]. Their corresponding acx2-1/3-6 double mutants have shorter roots than Col-0 plants when grown on sucrose-free medium due to the accumulation of long-chain acyl-CoAs[48,78]. As shown in Supplementary Fig. 17, *acx2-1/3-6* also had shorter roots than did Col-0 on the LP medium, and C2 inoculation effectively alleviated this phenomenon; in addition, C2 inoculation repressed the expression of *ACX2* family members in rapeseed roots, indicating that C2 is involved in the metabolism of acyl-CoA in plants. The affected JA biosynthesis may contribute to the colonization of C2 bacteria within the root system of rapeseed plants. Notably, similar to other *Flavobacterium* species such as the *Flavobacterium* humi sp. nov[79]. and *Flavobacterium baculatum* sp. nov[80]., C2 is a flexirubin-type pigment-producing bacterium that is yellow or orange in color at different pH values (Fig. 3f). Flexirubin is known as a yellow pigment that effectively protects against reactive oxygen species damage[80] and thus helps C2 in its symbiosis with the plant, whereas polyene chains in chromophore groups are synthesized from acetates in a manner similar to fatty acid biosynthesis[81]. Therefore, C2 may have the ability to
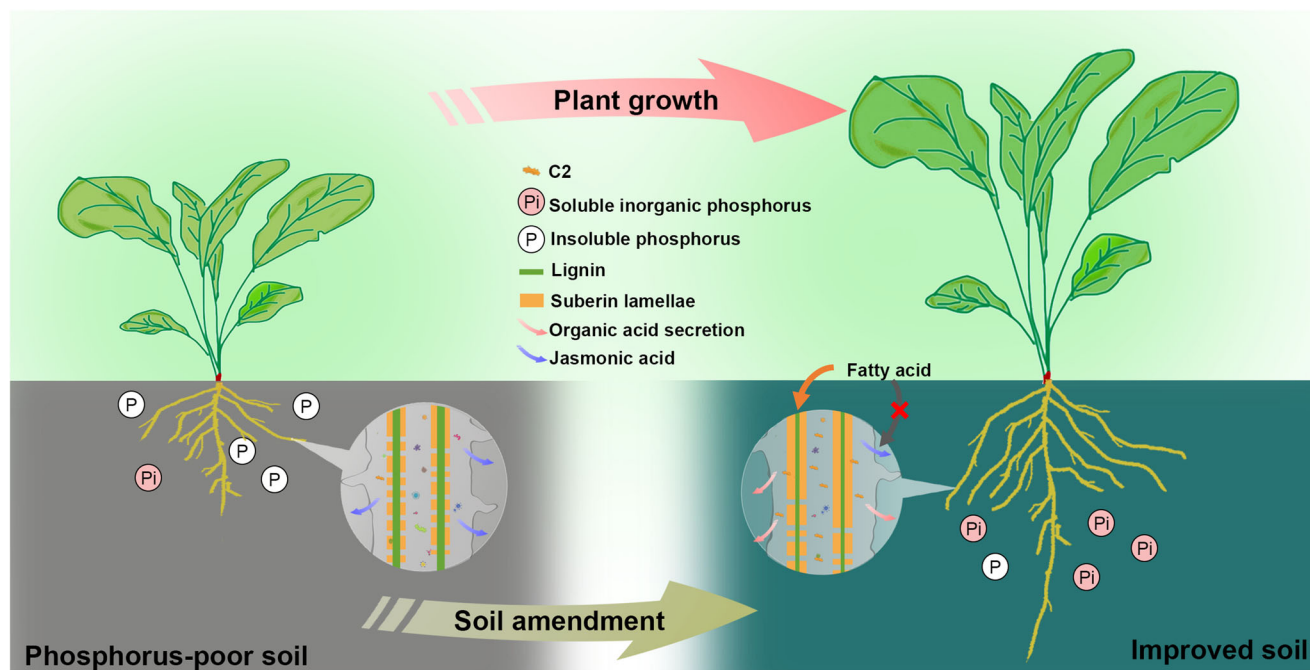
Fig. 6 | Proposed model for *Flavobacterium* C2-mediated plant growth and soil amendment. Phosphorus-soluble *Flavobacterium* C2 can effectively alleviate vegetative growth constraints in low-phosphorus environments by affecting the redistribution of lipids in the roots of *Brassica napus* L.

synthesize and metabolize fatty acids, resulting in a competitive relationship between C2 and rapeseed plants for JA biosynthesis process. Many classical studies on the stress response of cash crops have also reported that JA can act antagonistically to abscisic acid (ABA)[82], and endodermal suberization in *Arabidopsis* is positively correlated with ABA content[83]. The targeted metabolomics data showed that C2 inoculation effectively increased the ABA content in lateral roots under LP conditions (Fig. 5d).

In general, under low P conditions, rapeseed seedings decreased the deposition of suberin in their roots to promote P uptake by roots. However, the significantly increased lignification level and the accumulation of JA, starch, and other products limited the elongation of lateral roots in LP conditions. The phosphorus-solubilizing bacterium C2 can release organic acids into the soil to enhance P solubility and increase the content of Pi in the soil. Moreover, C2 reconstructed the α-linolenic acid metabolism-mediated JA and suberin biosynthesis network in roots, which improved C2 colonization and the vegetative growth of rapeseed (Fig. 6).

Methods

Plant materials and sample collection for the field experiment in Shilin, China

All the rapeseed cultivars were planted in Shilin of Yunnan Province (E:103°30′, N:24°81′), as shown in Supplementary Fig. 1. On the selected site, P fertilizer had not been applied for at least in the past 5 years prior to planting. This area was used for the P deficiency experimental group (low P[LP], phosphorus content: 9.01 mg/kg on average before planting). The other half of the site was treated with $Ca(H_2PO_4)_2$ to increase the soil P content to 19.93 mg/kg on average before planting, and this area was used for the control group (CK). Furthermore, urea, potassium chloride and borax were applied to the entir site to ensure the growth of rapeseed plants. Fifty plants foreach cultivar were grown in each plot (Supplementary Fig. 1; two replicates of CK or LP plots). The lateral roots of the rapeseeds (seedling stage, 30 days after germination) were washed twice with purified water, the surface moisture was removed, and the roots were immediately frozen in liquid nitrogen and then stored at −80 °C for RNA and DNA extraction.

Determination of nutrient contents

The ammonium molybdate spectrophotometric method was used to determine the P content of the soil. The contents of other nutrients were analyzed by inductively coupled plasma optical emission spectroscopy (ICP–OES, Thermo Scientific iCAP 6000 Series Cambridge, UK). For each plot, all 50 cultivars were analyzed, with 1–2 biological replicates per plot.

Transcriptome analysis

Total RNA was extracted from the tissue using TRIzol® Reagent according to the manufacturer's instructions (Invitrogen), and genomic DNA was removed using DNase I (TaKaRa). Then, RNA quality was determined with a 2100 Bioanalyzer (Agilent) and quantified using an ND-2000 (NanoDrop Technologies). Only high-quality RNA samples (OD260/280 = 1.8 ~ 2.2, OD260/230 ≥ 2.0, RNA integrity number [RIN] ≥ 8.0, 28S:18S ≥ 1.0, >1 μg) were used to construct the sequencing library. The RNA-seq transcriptome library was prepared using a TruSeq™ RNA Sample Preparation Kit from Illumina (San Diego, CA) with 1 μg of total RNA. Briefly, poly(A)+ messenger RNA was isolated with oligo(dT) beads and then fragmented using fragmentation buffer. Second, double-stranded cDNA was synthesized using a SuperScript double-stranded cDNA synthesis kit (Invitrogen, CA) with random hexamer primers (Illumina). Then, the synthesized cDNA was subjected to end repair, phosphorylation and A tailing according to Illumina's library construction protocol. Libraries were size selected for cDNA target fragments of 300 bp on 2% Low Range Ultra Agarose followed by PCR amplification using Phusion DNA polymerase (NEB) for 15 PCR cycles. After quantification by TBS380, the paired-end RNA-seq library was sequenced with an Illumina NovaSeq 6000 sequencer (2 × 150 bp read length). The raw paired-end reads were trimmed and quality controlled by fastp (version 0.19.5, https://github.com/OpenGene/fastp)[84] with default parameters. Then, the clean reads were separately aligned to the reference genome in orientation mode using HISAT2 (version 2.1.0, http://ccb.jhu.edu/software/hisat2/index.shtml) software. The expression level of each transcript was calculated according to the transcripts per million reads (TPM) method using RSEM (version 1.3.1, http://deweylab.biostat.wisc.edu/rsem/)[85].

Differentially expressed genes were determined according to a FDR ≤ 0.001 together with an absolute value of $\log_2$ (relative expression level) ≥1.

DNA extraction and Illumina MiSeq sequencing

Total DNA was extracted using and E.Z.N.A.® Soil DNA Kit (Omega Biotek, Norcross, GA, U.S.) according to the manufacturer's protocol. All DNA samples were quality checked, and their concentrations were quantified by NanoDrop 2000 spectrophotometers (Thermo Fisher Scientific, Wilmington, DE, USA). Bacterial 16S rRNA gene fragments (V3–V4) were amplified from the extracted DNA using primers 338 F (5′-ACTCCTACGGGAGGCAGCAG-3′) and 806 R (5′-GGACTACHVGG GTWTCTAAT-3′) and the following PCR conditions: 30 s at 95 °C, 30 s at 55 °C, and 45 s at 72 °C for 27 cycles. PCRs were performed with 4 μL 5 × TransStart FastPfu buffer, 2 μL 2.5 mM deoxynucleoside triphosphates (dNTPs), 0.8 μL of each primer (5 μM), 0.4 μL TransStart FastPfu DNA Polymerase, 10 ng of extracted DNA, and ddH2O to make up 20 μL. Agarose gel electrophoresis was performed to verify the size of the amplicons. Amplicons were subjected to paired-end sequencing on the Illumina MiSeq platform using PE300 chemistry at Majorbio Bio-Pharm Technology Co. Ltd. (Shanghai, China).

Amplicon sequence processing and analysis

After demultiplexing, the resulting sequences were merged with FLASH (v1.2.11) and quality filtered with fastp (0.19.6)[84,86]. Then, the high-quality sequences were denoised using the DADA2[87] plugin of the QIIME2[88] (version 2020.2) pipeline with recommended parameters, providing single-nucleotide resolution based on error profiles within samples. DADA2 denoised sequences are usually called amplicon sequence variants (ASVs). To minimize the effects of sequencing depth on alpha and beta diversity, the number of sequences from each sample was rarefied to 4000, which still yielded an average Good's coverage of 97.90%. Taxonomic assignment of ASVs was performed using the q2-feature-classifier and a naive Bayes taxonomy classifier against the SILVA 16S rRNA database (v138)[89,90]. ASVs assigned to mitochondria or chloroplast sequences were excluded. The remaining sequences, comprising only features with > 10 reads in ≥ 2 samples, were retained to assemble an ASV table. Analyses of the 16S rRNA microbiome sequencing data was performed using the free Majorbio Cloud Platform (www.majorbio.com). The similarity among microbial communities in different samples was assessed through principal coordinate analysis (PCoA) based on Bray-Curtis dissimilarity, implemented using the R Vegan package (v2.6-4).

Weighted gene co-expression network analysis (WGCNA)

To discern gene modules with distinct expression patterns and reveal correlations among the quantitative datasets, the WGCNA R package (v1.72.1) was employed. WGCNA, an unsupervised analysis method, was used to cluster genes based on their expression profiles across our 50 rapeseed zone-specific samples. For the robust construction of coexpression networks, we filtered genes with ≥ 10 mapped reads in at least two rapeseeds within corresponding zones. Gene expression data were normalized using transcripts per million (TPM) expression, and a total of 17,208 genes were utilized for module construction. Construction of a weighted coexpression network requires the soft-thresholding power value β, which was calculated by the pick Soft Threshold function of the R package[91]. We chose a power of 16, which is the lowest power for which the scale-free topology fit index curve flattens out, reaching a high value (above 0.98). To mitigate noise and false associations, we transformed adjacencies into a topological overlap matrix (TOM) and computed the corresponding dissimilarities (dissTOM), represented as 1−TOM. For hierarchical clustering of genes, dissTOM was employed as a distance measure. The minimum module size (i.e., number of genes) was set to 30, with a merge cut height of 0.25 to detect modules. A total of 16,317 genes (with a coefficient of variation of average RPM (CV > 1) among all samples) were assigned to 24 modules. To identify modules of interest that were highly related to the differentiation of P, SD, RD and ABS, a correlation analysis was conducted between each module and the ASVs. This relationship was determined by calculating the Spearman's correlation coefficient between module eigengenes (MEs, the major component of gene expression in a module) and differentiation traits. Modules showing significant correlations with differentiation traits were selected for further validation.

Biological function and gene set enrichment analyses

To investigate the biological functions of the differentiation-related modules, we performed enrichment analysis, including Gene Ontology (GO) term and Kyoto Encyclopedia of Genes and Genomes (KEGG) pathway enrichment analyses[92,93]. Functional GO functional enrichment analysis was conducted using Goatools (https://github.com/tanghaibao/goatools)[94], whereas KEGG pathway enrichment analysis was carried out using KOBAS[95].

Strain screening and functional verification

The method used to screen strain was described by Bai et al.[42]. A total of 0.1 g of each 16S sequencing sample was cut and mixed for *Flavobacterium* strain screening. A total of 378 ASVs (corresponding to 207 genera) were identified, and 7 of which were *Flavobacterium*. The four ASVs were further cultured on solid tryptone soy broth (TSB) medium. For the soil culture experiment, the rapeseed seeds were first pregerminated on CK + C2 solid medium for 48 h, then transferred to ground and sterilized soil (collected from Shi Lin, with 6.25 ppm P content; pot size: top 58 × 58 mm/bottom 20 × 20 mm/depth 110 mm, one plant per pot) and irrigated with ddH2O. Before bacterial inoculation, the bacteria were collected by centrifugation, the supernatant fermentation liquid was poured off, and the OD at 600 nm (OD600) was resuspended in CK or LP fluid medium to 0.8. On the 7th day after germination, 5 mL of the suspension solution was inoculated in each pot, followed by a weekly 5 mL supplement. The phenotype was recorded, and the plants were sampled 3 weeks after germination. The surfaces of the rapeseeds were sterilized with 70% (v/v) ethanol and 10% (w/v) sodium hypochlorite, rinsed with sterile water three times, germinated and grown on CK or LP (with 625 μM or 12.5 μM KH2PO4 added to the 1/2 MS base salts (-P, without vitamins)) solid medium supplemented with C2 (OD600 = 0.5, the inoculation volume was 1/40 of the medium volume) or an equal volume of ddH2O (as mock control). The growth conditions were 22–24 °C, under a long-day photoperiod (16-h light/8-h dark) and a relative humidity of 75% and a light intensity of 20000 Lux.

Scanning electron microscopy

The lateral roots of ZS11 were treated according to the methods of Jiang[96], and scanning electron microscopy (JSM-5610, Phenom, Holland, 10 kV) was used to characterize the colonization ability of C2 in the lateral roots of ZS11.

Laser scanning confocal microscopy for C2 colonization

C2 was grown at 28 °C in LB medium to OD600 = 0.6, diluted to OD600 = 0.3 with new medium containing 0.1 mM TRITC-d-Lys (Bioluminor, Ex: 560 nm; Em:580 nm), and then further incubated at 28 °C to OD600 = 1.42. The labeled bacteria were centrifuged and washed with fresh LB medium without TRITC-d-Lys three times. The roots of sterile transgenic (*35S::GFP*, Ex: 488 nm; Em: 510 nm) ZS11 seedlings were immersed in the above suspension solution for 72 h at 28 °C. The roots were washed three times with ddH2O before laser scanning confocal microscopy (LSM800, Zeiss, Germany) was performed.

Plant RNA extraction and real-time RT–qPCR

TRIzol reagent (TAKARA, Japan) was used to extract total RNA, with a total quantity of 500 ng of total RNA employed for reverse

transcription using the Transcriptor First Strand cDNA Synthesis Kit (TAKARA, Japan). The cDNA was diluted 10 times and then used as a template for quantitative PCR (RT–qPCR). qPCR was performed on an RT–PCR system (Thermo Fisher 7500) included 0.2 μL of PCR forward primer (10 μM), 5 μL of SYBR® Premix Ex TaqTM (2×), 1 μL of cDNA template, 0.2 μL of PCR reverse primer (10 μM), and distilled and deionized water up to 10 μL. The primers used for RT–qPCR are listed in Supplementary Data 12.

Bacterial genome sequencing and assembly

Bacterial strain C2 was streaked onto LB solid medium and cultured at 37 °C for 12 h. Next, a single colony on solid medium was inoculated into 200 mL of LB liquid medium and cultured at 37 °C for -12 h at 150 rpm. The cell biomass was harvested after 10 min centrifugation at 12,000 × g. Genomic DNA from C2 was extracted using a Wizard® Genomic DNA Purification Kit (Promega) according to the manufacturer's protocol. Purified genomic DNA was quantified by a TBS-380 fluorometer (Turner BioSystems Inc., Sunnyvale, CA). The genome was sequenced using a combination of Illumina NovaSeq 6000 and Nanopore PromethION sequencing platforms. Illumina data were used to evaluate genome complexity.

For Illumina sequencing, at least 1 μg of extracted *Flavobacterium* C2 genomic DNA was used for each strain for sequencing library construction. Genomic DNA samples were sheared into 400–500 bp fragments using a Covaris M220 focused acoustic shearer following the manufacturer's protocol. Illumina sequencing libraries were prepared from the sheared fragments using a NEXTflex™ Rapid DNA-Seq Kit. Briefly, the 5′ ends were first end-repaired and phosphorylated. Next, the 3′ ends were A-tailed and ligated to sequencing adapters. The third step was to enrich the adapter-ligated products using PCR. The prepared libraries were then subjected to paired-end Illumina sequencing (2 × 150 bp) on an Illumina NovaSeq 6000 platform (Illumina, San Diego, CA, USA).

For Nanopore sequencing, -10 μg of *Flavobacterium* C2 genomic DNA was isolated and size-selected using BluePippin (Sage Science, Beverly, MA, USA) and processed according to the (1D) Ligation Sequencing Kit (SQK-LSK109) protocol. Briefly, DNA fragments were end-repaired using NEBNext FFPE Repair Mix (New England Biolabs). After end repair and 3′-adenylation with NEBNext End Repair/dA-Tailing Module reagents (New England Biolabs), sequencing adapters supplied in the SQK-LSK109 kit were ligated to the DNA ends. The final library was loaded onto an R9.4 flow cell in a PromethION DNA sequencer (Oxford Nanopore, Oxford, UK) and sequenced for 48 h.

The data generated from the Nanopore and Illumina platforms were used for bioinformatics analysis. All of the analyses were performed using the free Majorbio Cloud Platform (http://cloud.majorbio.com) from Shanghai Majorbio Biopharm Technology Co., Ltd. The detailed procedures are as follows.

The raw Illumina sequencing reads generated from the paired-end library were subjected to quality filtering using fastp v0.23.0. Nanopore reads were extracted, basecalled and demultiplexed, and trimmed using ONT Guppy with a minimum Q score cutoff of 7. Then, the clean short and long reads were coassembled to construct complete genomes using Unicycler v0.4.8. As a final step, Unicycler uses Pilon v1.22 to polish the assembly using short-read alignments, reducing the rate of small errors. The coding sequences (CDSs) of chromosomes and plasmids were predicted using Prodigal v2.6.3[97] and GeneMarkS[98], respectively. tRNA-scan-SE (v 2.0)[99] was used for tRNA prediction, and Barrnap v0.9 (https://github.com/tseemann/barrnap) was used for rRNA prediction. The predicted CDSs were annotated from the NR, Swiss-Prot, Pfam, GO, COG and KEGG databases using sequence alignment tools such as BLAST, Diamond and HMMER. Briefly, each set of query proteins was aligned with the databases, and annotations of the best-matched subjects (*e*-value < 10⁻⁵) were obtained for gene annotation.

Average nucleotide identity analysis

Average nucleotide identity (ANI) analysis was performed with the online page server JSpeciesWS (https://jspecies.ribohost.com/jspeciesws/#home) and calculated based on BLAST+ (ANIb). The genome sequences of the strains were obtained from the search results of the GenomeDB tools.

Bacterial culture experiments

Conventional bacterial culture was performed using LB medium with shaking at 220 rpm and at 28 °C. The insoluble phosphate medium included sucrose 10 g, $(NH_4)_2SO_4$ 0.5 g, $MgSO_4·7H_2O$ 0.3 g, NaCl 0.3 g, KCl 0.3 g, $FeSO_4·7H_2O$ 0.03 g, $MnSO_4·7H_2O$ 0.03 g, $Ca_3(PO_4)_2$ 5 g, and agar 20 g, brought to a final volume of 1 L with distilled water; the pH was 7.2, and the solution was sterilized by autoclaving at 121 °C for 20 min. The Salkowski colorimetric solution consisted of 1 mL of 0.5 M $FeCl_3$ and 50 mL of 35% (w/v) $HClO_4$.

Quasitargeted metabolomics

Root tissues (100 mg) were individually ground in liquid nitrogen, and the homogenate was resuspended in prechilled 80% (v/v) methanol by vortexing. A total of 12 test samples (4 groups, 3 biological replicates for each group) were incubated on ice for 5 min and then centrifuged at 15,000 × g and 4 °C for 20 min. Some of the supernatant was diluted to a final concentration of 53% methanol with LC–MS grade water. The samples were subsequently transferred to a fresh Eppendorf tube and then centrifuged at 15000 × g and 4 °C for 20 min. Finally, the supernatant was injected into the LC–MS/MS system for analysis[100]. LC–MS/MS analysis was performed using an ExionLCTM AD system (SCIEX) coupled with a QTRAP® 6500+ mass spectrometer (SCIEX) by Novogene Co., Ltd. (Beijing, China). The samples were injected onto an Xselect HSS T3 (2.1 × 150 mm, 2.5 μm) using a 20 min linear gradient at a flow rate of 0.4 mL/min in positive/negative polarity mode. The eluents were eluent A (0.1% [v/v] formic acid–water) and eluent B (0.1% [v/v] formic acid–acetonitrile). The solvent gradient was set as follows (all percentages in v/v): 2% B, 2 min; 2–100% B, 15.0 min; 100% B, 17.0 min; 100–2% B, 17.1 min; and 2% B, 20 min. A QTRAP® 6500+ mass spectrometer was operated in positive polarity mode with a curtain gas of 35 psi, a collision gas setting of medium, and ion spray voltage of 5500 V, a temperature of 550 °C, an ion source gas of 1:60, and an ion source gas of 2:60. The QTRAP® 6500+ mass spectrometer was also operated in negative polarity mode with a curtain gas of 35 psi, a collision gas setting of medium, an ion spray voltage of −4500 V, a temperature of 550 °C, an ion source gas of 1:60, and an ion source gas of 2:60. The detection of the experimental samples in multiple reaction monitoring mode was based on an in-house Novogene database. Q3 was used for metabolite quantification. Q1, Q3, RT (retention time), DP (declustering potential) and CE (collision energy) were used for metabolite identification. The data files generated by HPLC–MS/MS were processed using SCIEX OS Version 1.4 to integrate and correct the peaks. The main parameters were set as follows: minimum peak height, 500; signal/noise ratio, 5; Gaussian smooth width, 1. The area of each peak represents the relative content of the corresponding substance.

Genome-wide association study

GWAS was performed with the online server BnaGWAS (http://121.41.229.126:3838/gwas/#tab-8340-1) using the EMMAX model[101]. A total of 13,573 high-confidence SNPs (missing data < 50%, minor allele frequency [MAF] > 5%) were identified by comparing the 50 rapeseed genomes with the reference genome from "Darmor-bzh". GWAS identified 18 significant SNPs (-log10 *P*-value > 5) linked to 221 genes (within a distance of 75 kb) that are associated with *Flavobacterium* ASV abundance variation in LP relative to CK conditions, based on the value of $\log_2$ (fold-change [average LP1, LP2/average CK1, CK2]) from the 50 rapeseed cultivars.

Targeted metabolomics

Liquid chromatography was performed on a Nexera UHPLC LC-30A (SHIMADZU). An ACQUITY UPLC HSS T3 (100 mm × 2.1 mm, 1.8 μm) was used for analysis. All samples were kept at 4 °C during the analysis, and the column temperature was set at 40 °C. Mass spectrometry was performed on an AB SCIEX Selex ION Triple Quad™ 5500 System with an electrospray ionization (ESI) source operating in both positive and negative ion modes. Nitrogen was employed as the collision gas. The targeted metabolites were analyzed in multiple reaction monitoring (MRM) mode. The multiple reaction monitoring (MRM) pairs, DPDPs and CEs were optimized for each analyte. Data acquisition and further analysis were conducted using Analyst software. SCIEX OS-MQ software was used to quantify all metabolites.

Suberin and lignin staining of lateral roots

The staining of suberin or lignin in roots was performed according to a previous method with Fluorol Yellow (FY 088, Santa Cruz Biotechnology) or basic fuchsin staining with aniline blue counterstaining[102,103]. Fluorescence images were captured using a confocal laser scanning microscope (LSM78010800; Zeiss780). The excitation and detection windows used were set as follows: GFP, excitation, 488 nm, emission, 510 nm; mCherry, excitation, 588 nm, emission, 1610 nm. ImageJ was used to quantify the fluorescence intensity of GFP and mCherry. To eliminate the effect of root length on suberin, Arabidopsis seedlings were grown on solid culture medium with their roots shaded[104,105].

Statistics and reproducibility

In this study, we initially selected 272 materials with relatively distant genetic relationships (provided by the Institute of Crop Science, Zhejiang University) for field trials. Ultimately, 50 core cultivars were retained for subsequent sampling by excluding those with inconsistent phenotypes between the two control plots or the two LP plots. Aside from this specific design, no data in this article were excluded from the analysis The experiments were not randomized, and the investigators were not blinded to the allocation during the experiments and outcome assessments. We believe that these methods ensure the reproducibility of our findings.

Reporting summary

Further information on research design is available in the Nature Portfolio Reporting Summary linked to this article.

Data availability

The RNA-seq data generated in this study were deposited to the NCBI Sequence Read Archive database under accession number PRJNA975333: https://www.ncbi.nlm.nih.gov/bioproject/PRJNA975333/. All 16S short-read data have been submitted to the NCBI and can be accessed through BioProject PRJNA997085: https://www.ncbi.nlm.nih.gov/bioproject/?term=PRJNA997085. Genome information for C2 been uploaded to Figshare and can be accessed via https://doi.org/10.6084/m9.figshare.27152274.v1. Quasitargeted metabolome data generated in this study are provided in the Supplementary Data 9 and 10. The metabolomics data have been uploaded to Figshare and can be accessed via https://doi.org/10.6084/m9.figshare.24580753.v1. Source data are provided with this paper.

References

1. Herrera-Estrella, L. & López-Arredondo, D. Phosphorus: The underrated element for feeding the world. *Trends Plant Sci.* **21**, 461–463 (2016).
2. Plaxton, C. W. & Shane, M. W. *Annual Plant Reviews Volume 48: Phosphorus Metabolism in Plants,* Vol. 48 (Wiley & Sons, 2015).
3. Adu, M. O. et al. A scanner-based rhizobox system enabling the quantification of root system development and response of Brassica rapa seedlings to external P availability. *Plant Root* **11**, 16–32 (2017).
4. Vance, C. P., Uhde-Stone, C. & Allan, D. L. Phosphorus acquisition and use: critical adaptations by plants for securing a nonrenewable resource. *N. Phytol.* **157**, 423–447 (2010).
5. López-Arredondo, D. L., Leyva-González, M. A., González-Morales, S. I., López-Bucio, J. & Herrera-Estrella, L. Phosphate nutrition: improving low-phosphate tolerance in crops. *Annu. Rev. Plant Biol.* **65**, 95–123 (2014).
6. Zhou, M. et al. Proteomic analysis dissects molecular mechanisms underlying plant responses to phosphorus deficiency. *Cells* **11**, 651 (2022).
7. Oldroyd, G. E. D. & Leyser, O. A plant's diet, surviving in a variable nutrient environment. *Science* **368**, eaba0196 (2020).
8. Młodzińska, E. & Zboińska, M. Phosphate uptake and allocation – a closer look at arabidopsis thaliana L. and oryza sativa L. *Front. Plant Sci.* **7**, 1198 (2016).
9. Wang, Y., Wang, F., Lu, H., Liu, Y. & Mao, C. Phosphate uptake and transport in plants: an elaborate regulatory system. *Plant Cell Physiol.* **4**, 564–572 (2021).
10. Duan, K. et al. Characterization of a sub-family of Arabidopsis genes with the SPX domain reveals their diverse functions in plant tolerance to phosphorus starvation. *Plant J. Cell Mol. Biol.* **546**, 965–975 (2008).
11. Shi, J. et al. The paralogous SPX3 and SPX5 genes redundantly modulate Pi homeostasis in rice. *J. Exp. Bot.* **65**, 859–870 (2014).
12. Stefanović, A. et al. Over-expression of PHO1 in Arabidopsis leaves reveals its role in mediating phosphate efflux. *Plant J. Cell Mol. Biol.* **66**, 689–699 (2011).
13. Liu, T.-Y. et al. Identification of plant vacuolar transporters mediating phosphate storage. *Nat. Commun.* **7**, 11095 (2016).
14. Wang, C. et al. Rice SPX-major facility superfamily3, a vacuolar phosphate efflux transporter, is involved in maintaining phosphate homeostasis in rice1[OPEN]. *Plant Physiol.* **169**, 2822–2831 (2015).
15. Jie, K. et al. Physiological mechanisms behind differences in pod shattering resistance in rapeseed (Brassica napus L.) varieties. *PLoS ONE* **11**, e0157341 (2016).
16. Zhao Sheng, Z., Jian Bo, S. & Zhi Min, Y. Genome-wide identification of Brassica napus microRNAs and their targets in response to cadmium. *J. Exp. Bot.* **63**, 4597–4613 (2012).
17. Wang, B., Wu, Z. & Liu, K. Dissection of the genetic architecture of three seed-quality traits and consequences for breeding in Brassica napus. *Plant Biotechnol. J.* **16**, 1336–1348 (2018).
18. Lu, K., LiJuan, W. & Li, X. Whole-genome resequencing reveals Brassica napus origin and genetic loci involved in its improvement. *Nat. Commun.* **10**, 1154 (2019).
19. Wu, D., Zhe, L., Tao, Y., Ying, X. & Jiang, L. Whole-genome resequencing of a world-wide collection of rapeseed accessions reveals genetic basis of their ecotype divergence. *Mol. Plant* **12**, 30–43 (2018).
20. Zhi-Yu, L. I., Qiong, H. U., Xing, L., Qing-Yuan, G. & Ya-Ping, Q. Effects of nitrogen,phosphorus and boron on the yield and quality of high-efficient oilseed rape hybrid Zhongyouza 8. *Chin. J. Oil Crop Sci.* **27**, 59–63 (2005).
21. Taoxiong, S., ShaoSi, W., Lei, S., Jin-ling, M. & Fangsen, X. Effects of N,P,K and B fertilization on quality of Brassica napus high and double low rapeseed Brassica napus. *Plant Nutr. Fertil. Sci.* **16**, 959–964 (2010).
22. Zhao, Z. et al. Boron and phosphorus act synergistically to modulate absorption and distribution of phosphorus and growth of Brassica napus. *J. Agric. Food Chem.* **68**, 7830–7838 (2020).
23. Hardoim P. R. et al. The hidden world within plants: ecological and evolutionary considerations for defining functioning of microbial endophytes. *Microbiol. Mol. Biol. Rev.* **79**, 293–320 (2015).

24. Kogel K. H., Franken P., Hückelhoven R. Endophyte or parasite–what decides? *Curr. Opin. Plant Biol.* **9**, 358–363 (2006).

25. Ryan, R. P., Germaine, K., Franks, A., Ryan, D. J. & Dowling, D. N. Bacterial endophytes: recent developments and applications. *FEMS Microbiol. Lett.* **278**, 1–9 (2008).

26. Chang, P. et al. Plant growth-promoting Bacteria facilitate the growth of barley and oats in salt-impacted soil: implications for phytoremediation of saline soils. *Int. J. Phytoremediat.* **16**, 1133–1147 (2014).

27. Rho, H. et al. Do Endophytes promote growth of host plants under stress? a meta-analysis on plant stress mitigation by Endophytes. *Microb. Ecol.* **75**, 407–418 (2017).

28. Rilling, J. I. et al. Current opinion and perspectives on the methods for tracking and monitoring plant growth–promoting bacteria. *Soil Biol. Biochem.* **130**, 698491 (2018).

29. Bledsoe, R. B., Goodwillie, C. & Peralta, A. L. Long-term nutrient enrichment of an oligotroph-dominated wetland increases bacterial diversity in bulk soils and plant Rhizospheres. *mSphere* **5**, e00035–20 (2020).

30. Gomez, S. K. Assessment of local and systemic changes in plant gene expression and aphid responses during potato interactions with arbuscular mycorrhizal fungi and potato aphids. *Plants* **9**, 82 (2020).

31. Maryam, S. et al. Mitigation of NaCl stress by arbuscular mycorrhizal fungi through the modulation of osmolytes, antioxidants and secondary metabolites in mustard (Brassica juncea L.) plants. *Front. Plant Sci.* **7**, 2040 (2016).

32. Delavaux et al. Beyond nutrients: a meta-analysis of the diverse effects of arbuscular mycorrhizal fungi on plants and soils. *ECOLOGY* **2017**, 2111–2119 (2017).

33. Floc, H. et al. Long-term persistence of arbuscular mycorrhizal fungi in the rhizosphere and bulk soils of non-host. *Front. Plant Sci.* **13**, 828145 (2022).

34. Ryan, M. H. et al. Increasing mycorrhizal colonisation does not improve growth and nutrition of wheat on Vertosols in south-eastern Australia. *Aust. J. Agric. Res.* **53**, 1173–1181 (2002).

35. Chih-Wei, K. et al. A Chinese cabbage (Brassica campetris subsp. Chinensis) τ-type glutathione-S-transferase stimulates Arabidopsis development and primes against abiotic and biotic stress. *Plant Mol. Biol.* **92**, 643–659 (2016).

36. Lee. et al. Growth promotion of chinese cabbage and arabidopsis by piriformospora indica is not stimulated by mycelium-synthesized auxin. *Mol. Plant Microbe. Int.* **24**, 421–31 (2011).

37. Sheqin, D. et al. The maturation zone is an important target of piriformospora indica in Chinese cabbage roots. *J. Exp. Bot.* **64**, 4529–4540 (2013).

38. Wolde-Meskel, E. et al. Additive yield response of chickpea (Cicer arietinum L.) to rhizobium inoculation and phosphorus fertilizer across smallholder farms in Ethiopia. *Agric. Ecosyst. Environ.* **261**, 144–152 (2018).

39. Tian, Y. et al. Long-term soil warming decreases microbial phosphorus utilization by increasing abiotic phosphorus sorption and phosphorus losses. *Nat. Commun.* **14**, 864 (2023).

40. Siles, J. A. et al. Distribution of phosphorus cycling genes across land uses and microbial taxonomic groups based on metagenome and genome mining. *Soil Biol. Biochem.* **174**, 108826 (2022).

41. Xuan, L. et al. Genome-wide association study reveals new genes involved in leaf trichome formation in polyploid oilseed rape (Brassica napus L.). *Plant Cell Environ.* **43**, 675–691 (2020).

42. Zhang, J. et al. High-throughput cultivation and identification of bacteria from the plant root microbiota. *Nat. Protoc.* **16**, 988–1012 (2021).

43. Yadav, V. et al. ABCG transporters are required for suberin and pollen wall extracellular barriers in arabidopsis. *Plant Cell* **26**, 3569–3588 (2014).

44. Krishnamurthy, P., Vishal, B., Bhal, A. & Kumar, P. P. WRKY9 transcription factor regulates cytochrome P450 genes CYP94B3 and CYP86B1, leading to increased root suberin and salt tolerance in Arabidopsis. *Physiol. Plant.* **172**, 1673–1687 (2021).

45. Lee, S. B. et al. Two Arabidopsis 3-ketoacyl CoA synthase genes, KCS20 and KCS2/DAISY, are functionally redundant in cuticular wax and root suberin biosynthesis, but differentially controlled by osmotic stress. *Plant J.* **60**, 462–75 (2010).

46. Caitlin et al. Repression of jasmonate signaling by a non-TIFY JAZ protein in Arabidopsis. *Plant J.* **82**, 669–679 (2015).

47. Gao, Y. Q. et al. A dirigent protein complex directs lignin polymerization and assembly of the root diffusion barrier. *Science* **382**, 464–471 (2023).

48. Wen-Cheng et al. CATALASE2 functions for seedling post-germinative growth by scavenging H2 O2 and stimulating ACX2/3 activity in Arabidopsis. *Plant Cell Environ.* **40**, 2720–2728 (2017).

49. Zhu, J., Li, M. & Whelan, M. J. Phosphorus activators contribute to legacy phosphorus availability in agricultural soils: a review. *Sci. Total Environ.* **612**, 522–537 (2018).

50. Marra, L. M. et al. Initial pH of medium affects organic acids production but do not affect phosphate solubilization. *Braz. J. Microbiol.* **46**, 367–375 (2015).

51. Incremental acidification reveals phosphorus release dynamics in alkaline vertic soils. *Geoderma* **259**, 35–44 (2015).

52. Debnath, S. C. et al. Flavobacterium sharifuzzamanii sp. nov., isolated from the sediments of the East China sea. *Curr. Microbiol.* **76**, 297–303 (2018).

53. Li, H. et al. Multi-omics analysis of the regulatory effects of low-phosphorus stress on phosphorus transport in soybean roots. *Front. Plant Sci.* **13**, 992036 (2022).

54. Yuan, H. & Liu, D. Signaling components involved in plant responses to phosphate starvation. *J. Integr. Plant Biol.* **50**, 849–859 (2008).

55. Li, Y. et al. Local and systemic responses conferring adaptation of Brassica napus roots to low phosphorus conditions. *J. Exp. Bot.* **73**, 4753–4777 (2022). **14**.

56. Yao, Y., Sun, H., Xu, F., Zhang, X. & Liu, S. Comparative proteome analysis of metabolic changes by low phosphorus stress in two Brassica napus genotypes. *Planta* **233**, 523–537 (2011).

57. Ren, F. et al. A Brassica napus PHT1 phosphate transporter, BnPht1;4, promotes phosphate uptake and affects roots architecture of transgenic Arabidopsis. *Plant Mol. Biol.* **86**, 595–607 (2014).

58. Herrera, A. S. et al. Beyond mitochondria, what would be the energy source of the cell? *Cent. Nerv. Syst. Agents Med. Chem.* **151**, 32–41 (2015).

59. Liu, C. et al. Heterologous expression of the transcription factor EsNAC1 in arabidopsis enhances abiotic stress resistance and retards growth by regulating the expression of different target genes. *Front. Plant Sci.* **9**, 1495 (2018).

60. Inouhe, M., Hayashi, K. & Nevins, D. J. Polypeptide characteristics and immunological properties of exo- and endoglucanases purified from maize coleoptile cell walls. *J. Plant Physiol.* **154**, 334–340 (1999).

61. Bauer, vStefan, Vasu, P., Persson, S., Mort, A. J. & Somerville, C. R. Development and application of a suite of polysaccharide-degrading enzymes for analyzing plant cell walls. *Proc. Natl Acad. Sci. Usa.* **103**, 11417–11422 (2006).

62. Thakker, C., Martínez, I., Li, W., San, K.-Y. & Bennett, G. N. Metabolic engineering of carbon and redox flow in the production of small organic acids. *J. Ind. Microbiol. Biotechnol.* **42**, 403–422 (2015).

63. Baxter, I. R. et al. Root suberin forms an extracellular barrier that affects water relations and mineral nutrition in Arabidopsis. *PLoS Genet* **5**, e1000492 (2009).

64. Barberon, M. et al. Adaptation of root function by nutrient-Induced plasticity of endodermal differentiation. *Cell* **164**, 447–459 (2016).

65. Naseer, S. et al. Casparian strip diffusion barrier in Arabidopsis is made of a lignin polymer without suberin. *Proc. Natl Acad. Sci.* **109**, 10101–10106 (2012).

66. Marie & Barberon. The endodermis as a checkpoint for nutrients. *New Phytol.* **213**, 1604–1610 (2017).

67. Chen, A., Husted, S., Salt, D. E., Schjoerring, J. K. & Persson, D. P. The intensity of manganese deficiency strongly affects root endodermal suberization and ion homeostasis. *Plant Physiol.* **181**, 00507.2019 (2019).

68. Namyslov, J., Bauriedlová, Z., Janoušková, J., Soukup, A. & Tylová, E. Exodermis and endodermis respond to nutrient deficiency in nutrient-specific and localized manner. *Plants* **9**, 201 (2020).

69. Schneider, H. M. et al. Root cortical senescence decreases root respiration, nutrient content and radial water and nutrient transport in barley. *Plant Cell Environ.* **40**, 1392–1408 (2017).

70. Tyagi, W. & Rai, M. K. Root transcriptomes of two acidic soil adapted Indica rice genotypes suggest diverse and complex mechanism of low phosphorus tolerance. *Protoplasma* **254**, 725–736 (2017).

71. Alcock, T. D. et al. Species-wide variation in shoot nitrate concentration, and genetic loci controlling nitrate, phosphorus and potassium accumulation in Brassica napus L. *Front. Plant Sci.* **9**, 1487 (2018).

72. Qi, W. Z. et al. iTRAQ-based analysis of the Arabidopsis proteome reveals insights into the potential mechanisms of anthocyanin accumulation regulation in response to phosphate deficiency. *J. Proteom.* **184**, 39–53 (2018).

73. Wiszniewski, A. A. G., Bussell, J. D., Long, R. L. & Smith, S. M. Knockout of the two evolutionarily conserved peroxisomal 3-ketoacyl-CoA thiolases in Arabidopsis recapitulates the abnormal inflorescence meristem 1 phenotype. *J. Exp. Bot.* **65**, 6723–6733 (2014).

74. Afitlhile, M. M., Fukushige, H., Nishimura, M. & Hildebrand, D. F. A defect in glyoxysomal fatty acid β-oxidation reduces jasmonic acid accumulation in Arabidopsis. *Plant Physiol. Biochem.* **43**, 603–609 (2005).

75. Schilmiller, A. L., Koo, A. J. K. & Howe, G. A. Functional diversification of acyl-coenzyme a oxidases in jasmonic acid biosynthesis and action. *Plant Physiol.* **143**, 812–24 (2006).

76. Graham, I. A. & Eastmond, P. J. Pathways of straight and branched chain fatty acid catabolism in higher plants. *Prog. Lipid Res.* **41**, 156–181 (2002).

77. Adham, A. R., Zolman, B. K., Millius, A. & Bartel, B. Mutations in Arabidopsis acyl-CoA oxidase genes reveal distinct and overlapping roles in β-oxidation. *Plant J.* **41**, 859–874 (2005).

78. Helen et al. Sucrose rescues seedling establishment but not germination of Arabidopsis mutants disrupted in peroxisomal fatty acid catabolism. *Plant J.* **43**, 861–872 (2005).

79. Seo, C. T. Flavobacterium humi sp. nov., a flexirubin-type pigment producing bacterium, isolated from soil. *J. Microbiol.* **57**, 1079–1085 (2019).

80. Chhetri, G., Kim, J., Kim, I., Kang, M. & Seo, T. Flavobacterium baculatum sp. nov., a carotenoid and flexirubin-type pigment producing species isolated from flooded paddy field. *Int. J. Syst. Evol. Microbiol.* https://doi.org/10.1099/ijsem.0.004736 (2021).

81. Schoener et al. Initiation of the flexirubin biosynthesis in chitinophaga pinensis. *Microb. Biotechnol.* **7**, 232–241 (2014).

82. Jacobsen, J. V., Barrero, J. M., Hughes, T., Julkowska, M. & Gubler, F. Roles for blue light, jasmonate and nitric oxide in the regulation of dormancy and germination in wheat grain (Triticum aestivum L.). *Planta* **238**, 121–138 (2013).

83. Salas-González, I. et al. Coordination between microbiota and root endodermis supports plant mineral nutrient homeostasis. *Science* **371**, eabd0695 (2020).

84. Chen, S., Zhou, Y., Chen, Y. & Gu, J. fastp: an ultra-fast all-in-one FASTQ preprocessor. *Bioinformatics* **17**, 884–890 (2018).

85. Li, B. & Dewey, C. N. RSEM: accurate transcript quantification from RNA-Seq data with or without a reference genome. *BMC Bioinforma.* **12**, 93–99 (2011).

86. Magoc, T. & Salzberg, S. L. FLASH: fast length adjustment of short reads to improve genome assemblies. *Bioinformatics* **27**, 2957–2963 (2011).

87. Callahan, B. J. et al. DADA2: High resolution sample inference from amplicon data. *bioRxiv* **7**, 581–3 (2015).

88. Bolyen, E., Rideout, J. R., Dillon, M. R., Bokulich, N. A. & Caporaso, J. G. QIIME 2: Reproducible, interactive, scalable, and extensible microbiome data science. *Nat. Biotechnol.* **37**, 852–857 (2018).

89. Bokulich, N. A. et al. Optimizing taxonomic classification of marker-gene amplicon sequences with QIIME 2's q2-feature-classifier plugin. *Microbiome* **6**, 90 (2018).

90. Pelin, Y. et al. The SILVA and 'all-species living tree project (LTP)' taxonomic frameworks. *Nucleic Acids Res.* **42**, D643-8 (2013).

91. Langfelder, P. & Horvath, S. WGCNA: an R package for weighted correlation network analysis. *BMC Bioinforma.* **9**, 599 (2008).

92. Consortium, T. G. O. Gene ontology: tool for the unification of biology. *Nat. Genet.* **25**, 25–29 (2000).

93. Kanehisa, M. & Goto, S. KEGG: Kyoto encyclopedia of genes and genomes. *Nucleic Acids Res* **28**, 27–30 (2000).

94. Klopfenstein, D. V. et al. GOATOOLS: A python library for gene ontology analyses. *Sci. Rep.* **8**, 10872 (2018).

95. Dechao, B. et al. KOBAS-i: intelligent prioritization and exploratory visualization of biological functions for gene enrichment analysis. *Nucleic Acids Res.* **49**, W317–W325 (2021).

96. Jiang, L., Ling, S., Fu, M., Peng, C. & Zhou, B. Bioaccumulation, elimination and metabolism in earthworms and microbial indices responses after exposure to decabromodiphenyl ethane in a soil-earthworm-microbe system. *Environ. Pollut.* **289**, 117965 (2021).

97. Wick, R. R., Judd, L. M., Gorrie, C. L. & Holt, K. E. Unicycler: Resolving bacterial genome assemblies from short and long sequencing reads. *PLoS Comput. Biol.* **13**, e1005595 (2016).

98. Besemer, J. & Borodovsky, M. GeneMark: web software for gene finding in prokaryotes, eukaryotes and viruses. *Nucleic Acids Res.* **33**, W451–W454 (2005).

99. Chan, P. P. & Lowe, T. M. tRNAscan-SE: Searching for tRNA genes in genomic sequences. *Methods Mol. Biol.* **1962**, 1–14 (2019).

100. Want, E. J. et al. Global metabolic profiling of animal and human tissues via UPLC-MS. *Nat. Protoc.* **8**, 17–32 (2013).

101. Kang, H. M. et al. Variance component model to account for sample structure in genome-wide association studies. *Nat. Genet.* **42**, 348–354 (2010).

102. Ursache, R. et al. Discovery of GDSL-domain proteins as key players for suberin polymerization and degradation. *Nat. Plants* **7**, 353–364 (2021).

103. Manzano, C. et al. Regulation and function of a polarly localized lignin barrier in the exodermis. *bioRxiv* https://doi.org/10.1101/2022.10.20.513117 (2022).

104. Gao, Y. Q. et al. Long-distance blue light signalling regulates phosphate deficiency-induced primary root growth inhibition. *Mol. Plant* **14**, 1539–1553 (2021).

105. Zheng, Z., Wang, Z., Wang, X. & Liu, D. Blue light-triggered chemical reactions underlie phosphate deficiency-induced inhibition of root elongation of Arabidopsis seedlings grown in petri dishes. *Mol. Plant* **12**, 1515–1523 (2019).

Acknowledgements

Author contributions

N.L., C.L., X.C., D.W., P.Y., X.F., X.S., and L.J. designed and managed the project. C.L., Z.B., Y.L., Y.Z., Y.W., H.L., X.H., A.C., L.M., C.C., J.Y., Y.X., Y.Z., J.M., R.A., C.Y., H.C., J.C., Z.L., and X.L. collected samples and performed experiments. C.L., M.L., X.L., Y.D., J.Z., and N.L. performed data analyses. C.L., M.L. and N.L. wrote the manuscript. C.L., N.L., X.C., D.W., P.Y., X.F., X.S. and L.J. revised the manuscript.

Competing interests

The authors declare no competing interests.

Additional information

Correspondence and requests for materials should be addressed to Peng Yu, Daojie Wang, Xinping Chen or Nannan Li.

Reprints and permissions information is available at http://www.nature.com/reprints

Publisher's note Springer Nature remains neutral with regard to jurisdictional claims in published maps and institutional affiliations.

[1]College of Resources and Environment, and Academy of Agricultural Sciences, Southwest University, Chongqing 400715, China. [2]Interdisciplinary Research Center for Agriculture Green Development in Yangtze River Basin, Southwest University, Chongqing 400715, China. [3]Hybrid Rapeseed Research Center of Shaanxi Province, Yangling, Shaanxi 712100, China. [4]College of Agriculture, State Key Laboratory of Crop Stress Adaptation and Improvement, Henan University, Kaifeng 475004 Henan, China. [5]Shanghai Majorbio Research Institute, Shanghai 201203, PR China. [6]Crop Functional Genomics, Institute of Crop Science and Resource Conservation, University of Bonn, Bonn, Germany. [7]Institute of Crop Science, Zhejiang University, Hangzhou 310058, China. [8]Research Center for Intelligent Computing Platforms, Zhejiang Lab, Hangzhou 310012, China. [9]Plant Genetics, School of Life Sciences, Technical University of Munich, Freising D-85354, Germany. [10]Yazhouwan National Laboratory, Sanya 572025, China. [11]These authors contributed equally: Can Liu, Zhen Bai, Yu Luo, Yanfeng Zhang, Yongfeng Wang, Hexin Liu. ✉e-mail: yupeng@uni-bonn.de; wangdj@henu.edu.cn; chenxp2017@swu.edu.cn; linannan2013@swu.edu.cn